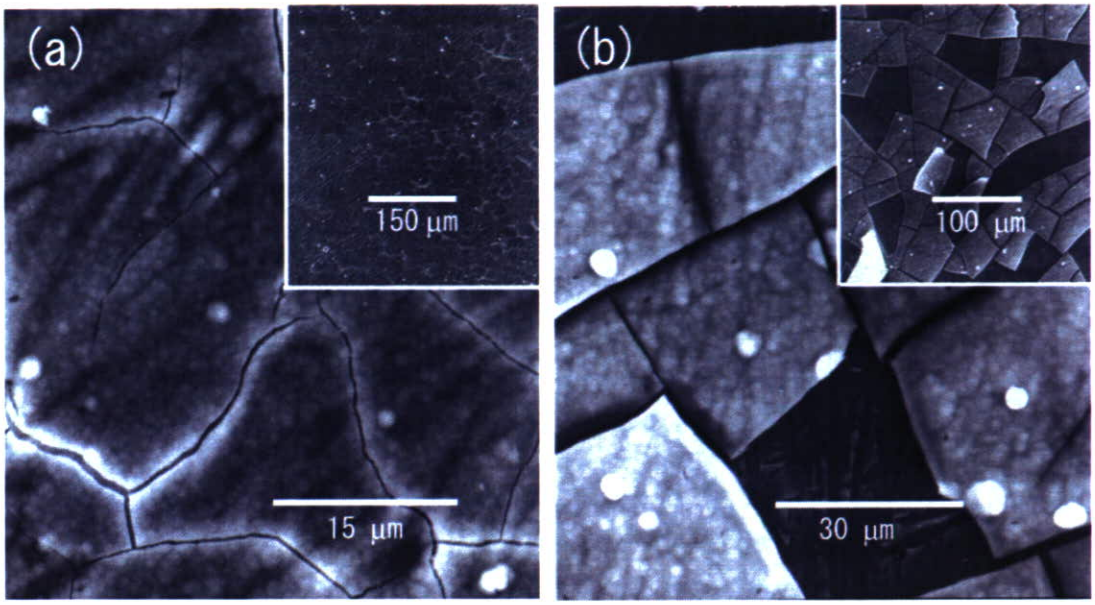

Fig. 5 SEM images for the surface after immersion in HBSS for 18 d: (a) unmodified-titanium surface, and (b) surface-modified-titanium surface. Inserted figures in upper quarter part are reduced SEM images.

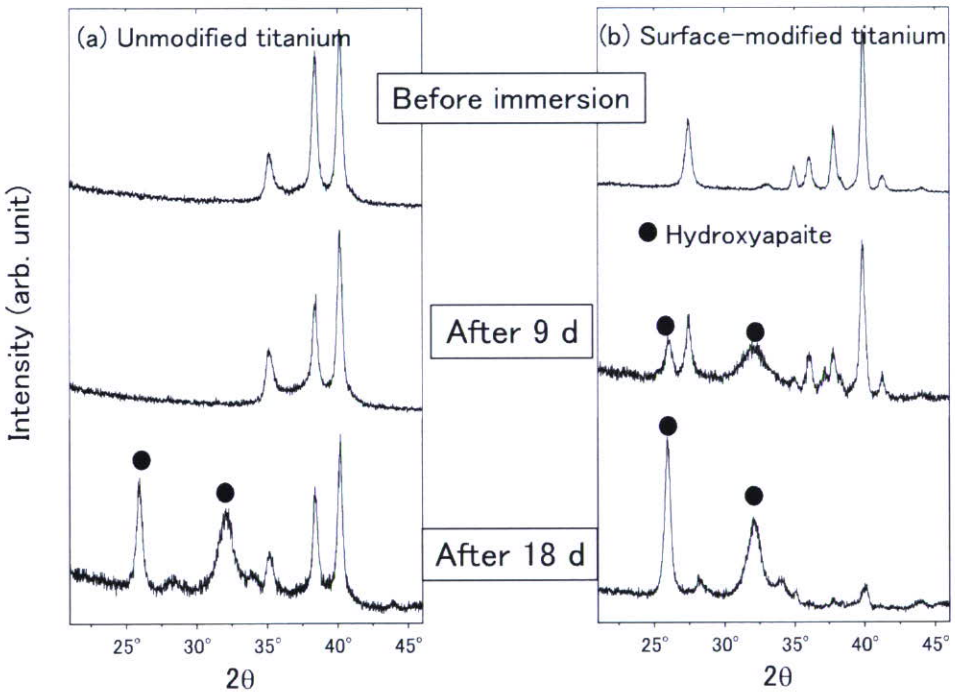

Fig. 6 GI-XRD patterns for (a) unmodified- and (b) surface-modified-titanium surfaces before and after immersion in HBSS for 9 and 18 d.

and surface-modified-titanium surface before and after immersion in HBSS for 9 and 18 d, respectively. New peaks appearing after the immersion are assigned to those of HAP. This result shows that the precipitates formed on the surfaces after the immersion are HAP. At 9 d, the peaks of HAP are observed only in the XRD patterns of the modified surface. This result corresponds to that of the SEM observation. At 18 d, the peaks of HAP are observed in the both modified and unmodified surface. On the other hand, the peaks of titanium are disappeared in the modified-surface XRD pattern because the thickness of the precipitate layer formed on the modified surface exceeds the effective depth of the GI-XRD. The result indicates that the thickness of the HAP layer formed on the modified surface is thicker than that on the unmodified surface and corresponds to the result of the SEM observation.

The results of the SEM and GI-XRD show that the formation speed of HAP layer on the surface-modified-titanium surface is much faster than that on the unmodified-

titanium surface. Thus, it is concluded that the performance of the calcium-phosphate formation in HBSS is improved by the calcium-hydroxide-slurry treatment. In general, surface which can form calcium phosphates rapidly is bioactive. Therefore, the calcium-hydride-slurry treatment is one of the promising treatments for improvement of bone conductivity.

4. Conclusion

By treating with newly developed calcium-hydroxide-slurry treatment, the surface of titanium changes to calcium-titanate layer with peroskite structure. Also, titanium-dioxide layer is formed under the calcium-titanate layer. The characteristics of the surface-modified titanium surface correspond to those of the calcium-titanate film prepared with radiofrequency magnetron sputtering and post-heating which can facilitate the bone formation. On the other hand, the interface between the modified layer and substrate is unclear, expected to give non-destructive interface. Speed of the hydroxyapatite formation on titanium in Hanks' balanced saline solution becomes faster by modifying with the calcium-hydroxide-slurry treatment, and thus, it is concluded that the treatment improve the performance of calcium-phosphate formation on titanium. The results show that the calcium-hydroxide-slurry treatment can modify titanium surface to a bioactive calcium-titanate layer with simple and low-cost, and it is indicated that the new technique is one of the promising treatments for improvement of bone conductivity.

Acknowledgment

The authors gratefully acknowledge Prof. K. Wagatsuma for supporting our research and Mr. Y. Murakami for teaching us SEM operation.

REFERENCES

1) A. Yamamoto, R. Honma and M. Sumita: J. Biomed. Mater. Res. **39** (1998) 331–340.
2) D. Kuroda, M. Niinomi, M. Morinaga, Y. Kato and T. Yashiro: Mater. Sci. Engng. A **A243** (1998) 244–249.
3) Y. Okazaki, S. Rao, T. Tateishi and Y. Ito: Mater. Sci. Engng. A **A243** (1998) 250–256.
4) Y. Okazaki, S. Rao, Y. Ito and T. Tateishi: Biomaterials **13** (1998) 1197–1215.
5) K. M. Speck and A. C. Fracker: J. Dent. Res. **59** (1980) 1590–1595.
6) Y. Nakayama, T. Yamamuro, Y. Kotoura and M. Oka: Biomaterials **10** (1989) 420–424.
7) Y. Okazaki and E. Gotoh: Biomaterials **26** (2005) 11–21.
8) K. De Groot, R. Geesink, C. P. Klein and P. Serekian: J. Biomed. Mater. Res. **21** (1987) 1375–1381.
9) J. H. C. Lin, M. L. Liu and C. P. Ju: J. Mater. Sci. Mater. Med. **5** (1994) 279–283.
10) F. Brossa, A. Cigada, R. Chiesa, L. Paracchini and C. Consonni: Biomed. Mater. Eng. **3** (1993) 127–136.
11) R. G. T. Geesink, K. de Groot and C. P. Klein: J. Bone. Joint Surg. **70B** (1988) 17–22.
12) S. R. Radin and P. Ducheyne: J. Mater. Sci. Mater. Med. **3** (1992) 33–42.
13) P. Ducheyne, S. Radin and L. King: J. Biomed. Mater. Res. **27** (1993) 25–34.
14) T. Hanawa, K. Murakami and S. Kihara: ASTM STP 1196, ed. By E. Horowita and J. E. Parr, (American Society for Testing and Materials, Philadelphia, 1994) pp. 170–184.
15) T. Hanawa, Y. Nodasaka, H. Ukai, K. Murakami and K. Asaoka: J. Jpn. Soc. Biomater. **12** (1994) 209–216.
16) T. Hanawa, H. Ukai and K. Murakami: J. Electron Spectrosc. **63** (1993) 347–354.
17) T. Hanawa, H. Ukai, K. Murakami and K. Asaoka: Mater. Trans. JIM **36** (1995) 438–444.
18) T. Hanawa, M. Kon, H. Ukai,bK. Murakami, Y. Miyamoto and K. Asaoka: J. Biomed. Mater. Res. **34** (1997) 273–278.
19) S. Nishiguchi, T. Nakamura, M. kobayashi, H.-M. Kim, F. Miyaji and T. Kokubo: Biomaterials **20** (1999) 491–500.
20) S. Nishiguchi, H. Kato, H. Fujita, H.-M. Kim, T. Kokubo and T. Nakamura: J. Biomed. Mater. Res. **54** (1999) 689–696.
21) S. Nishiguchi, H. Kato, H. Fujita, M. Oka, H.-M. Kim, T. Kokubo and T. Nakamura: Biomaterials **22** (2001) 2525–2533.
22) T. Kokubo, F. Miyaji, H.-M. Kim and T. Nakamura: J. Am. Ceram. Soc. **79** (1996) 1127–1129.
23) H.-M. Kim, F. Miyaji, T. Kokubo and T. Nakamura: J. Biomed. Mater. Res. **32** (1996) 409–417.
24) H. Takadama, H.-M. Kim, T. Kokubo and T. Nakamura: J. Biomed. Mater. Res. **55** (2001) 185–193.
25) H. Takadama, H.-M. Kim, T. Kokubo and T. Nakamura: J. Biomed. Mater. Res. **57** (2001) 441–448.
26) K. Asami, K. Saito, N. Ohtsu, S. Nagata and T. Hanawa: Surf. Inter. Anal. **35** (2003) 483–488.
27) N. Ohtsu, K. Sato, K. Saito T. Hanawa and K. Asami: Mater. Trans. JIM **45** (2004) 1778–1781.
28) N. Ohtsu, K. Saito, K. Asami and T. Hanawa: Surf. Coat. Tech. **200** (2006) 5455–5461.
29) N. Ohtsu, K. Sato, K. Saito, K. Asami and T. Hanawa: J. Mater. Sci. Mater. Med. (In press)
30) N. Ohtsu, K. Sato, A. Yanagawa, K. Saito, Y. Imai, T. Kohgo, A. Yokoyama, K. Asami and T. Hanawa: J. Biomed. Mater. Res. (In press)
31) K. Hamada, M. Kon, T. Hanawa, K. Yokoyama, Y. Miyamoto and K. Asaoka: Biomaterials **23** (2002) 2265–2272.
32) N. Ohtsu, T. Ashino and K. Asami: Mater. Trans. JIM **45** (2004) 550–553.
33) P. A. W. van der Heide: Surf. Sci. **490** (2001) L619–L626.

Materials Transactions, Vol. 48, No. 3 (2007) pp. 287 to 292
Special Issue on Smart and Harmonic Biomaterials

Determination of the Immobilization Manner of Amine-Terminated Poly(Ethylene Glycol) Electrodeposited on a Titanium Surface with XPS and GD-OES

Yuta Tanaka[1,*1], Hisashi Doi[1,*2], Equo Kobayashi[1], Takayuki Yoneyama[1,2] and Takao Hanawa[1]

[1]*Institute of Biomaterials and Bioengineering, Tokyo Medical and Dental University, Tokyo 101-0062, Japan*
[2]*Department of Materials Engineering, The University of Tokyo, Tokyo 113-8656, Japan*

Poly(ethylene glycol), PEG, is a biofunctional molecule that inhibits the adsorption of proteins. Therefore, the immobilization of PEG on a metal surface is an important step in making metal surfaces biofunctional. The bonding manner of PEG to a titanium surface is significant for the design of PEG-immobilized materials; however, there are few characterization techniques for the determination of the immobilization manner of PEG. In this study, PEG terminated at one or both terminals with amine bases was immobilized on a titanium surface with electrodeposition and immersion. The electrodeposition was carried out with −5 V for 300 s. The immobilization manner of PEG was characterized using X-ray photoelectron spectroscopy (XPS) with an angle-resolved technique and glow discharge optical emission spectroscopy (GD-OES). As a result, not only electrodeposition but also immersion led to the immobilization of PEG onto a titanium surface. However, more terminated amines combined with titanium oxide as an ionic NH-O with electrodeposition, while more amines randomly existed as NH_3^+ in the PEG molecule with immersion. Moreover, the difference in the amine termination resulted in a different manner of bonding. The PEG terminated at both terminals immobilized in a U shape, and the PEG terminated at one terminal immobilized a brush. Characterization with XPS and GD-OES is useful to determine the immobilization mode of PEG to a solid surface. [doi:10.2320/matertrans.48.287]

(Received August 22, 2006; Accepted November 10, 2006; Published February 25, 2007)

Keywords: *titanium, polyethylene glycol, immobilization, electrodeposition, surface analysis*

1. Introduction

Recently, biofunctions are required for metals. For example, stents are placed at stenotic blood vessels for dilatation, and blood compatibility or prevention of adhesion of platelets is necessary. Sliding lubrication in blood vessels is important when inserting guide wires and guiding catheters. In addition, if metals were to be used as sensing devices, the control of cell adhesion would be necessary. For these purposes, the fundamental property is the inhibition of protein adsorption. Poly(ethylene glycol), PEG, is a biofunctional molecule that inhibits the adsorption of proteins. Therefore, the immobilization of PEG to a metal surface is an important event to bio-functionalize a metal surface.

There are several stages in the process of immobilizing PEG on solid surfaces that have been recently studied. For example, the immobilization of PEG on silica or titanium surfaces consists of a two-stage reaction.[1)] In the first stage, an aminosilane or a thiosilane is reacted with a clean oxide surface to form a surface that is rich in amine or thiol functionalities. In the second stage, a PEG polymer that contains a functional group that is reactive with the modified surface is coupled to the surface. On the other hand, a certain amount of PEG is immobilized on titanium with electrodeposition when PEG is terminated by amine bases.[2)] The adsorption of albumin on a titanium surface is inhibited by immobilization. The technique is simple and universal for electroconductive materials and those with a complex morphology. However, the immobilization manner of PEG to a titanium surface with electrodeposition is not completely elucidated in the study referred to above.

In this study, PEG with both terminals or one terminal modified with amine bases was immobilized onto a titanium surface with electrodeposition. The immobilization manner and chemical bonding state were characterized using X-ray photoelectron spectroscopy (XPS) with an angle-resolved technique and glow discharge optical emission spectroscopy (GD-OES). This study will enhance the understanding of the electrodeposition of PEG on metals.

2. Materials and Methods

2.1 Electrodeposition

Both terminals of PEG were terminated with $-NH_2$ (PEG1000 Diamine, NOF Corporation, Japan), and only one terminal was terminated with $-NH_2$ (SUNBRIGHT MEPA-10H, NOF Corporation, Japan). The chemical structures of the PEGs are shown in Fig. 1. The molecular weights of both PEGs were about 1,000. These terminated PEGs were dissolved in a 0.3-mol L^{-1} NaCl solution as a concentration of 2 mass%. In the solution, the $-NH_2$ terminal was dissociated and positively charged as $-NH_3^+$. The pH of

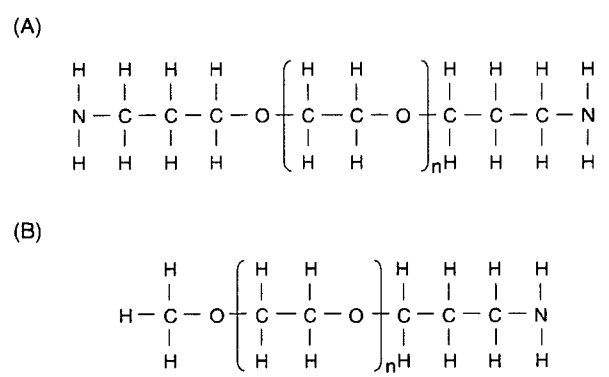

Fig. 1 Chemical structures of PEGs in which both terminals (A) and one terminal (B) were terminated with amine.

*1Graduate Student, Tokyo Medical and Dental University
*2Corresponding author, E-mail: doi.met@tmd.ac.jp

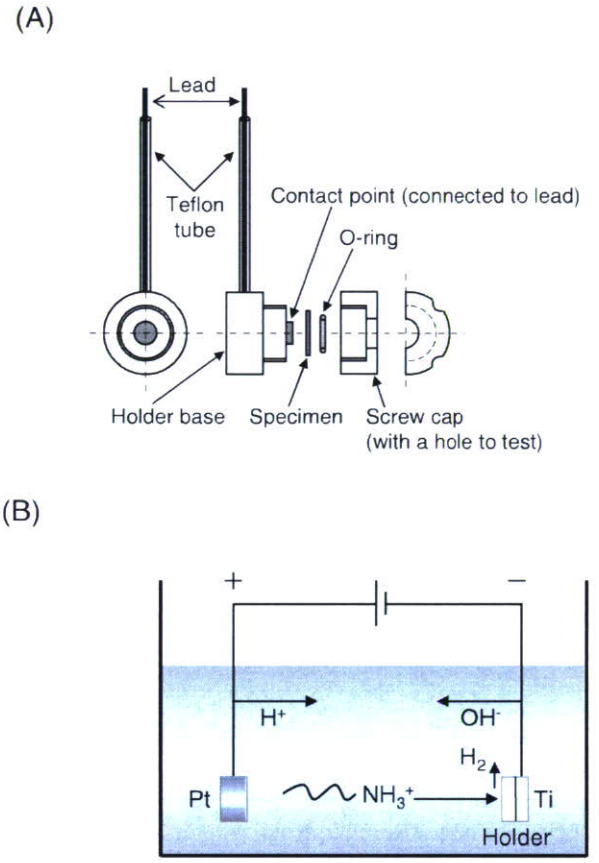

Fig. 2 Design of a polytetrafluoroethylene holder of titanium for electrodeposition (A) and schematic illustration of electrodeposition (B).

the PEG solution with both terminals modified was 11.2, and that of the solution with one terminal modified was 11.0. The resultant solution was used as an electrolyte for electrodeposition at 310 K.

A commercially pure titanium disk (8 mmϕ × 2 mm in thickness) with grade 2 was metallographically polished and ultrasonically rinsed in acetone and deionized water (Millipore). The titanium disk was fixed in a polytetrafluoroethylene holder that was completely insulated from the electrolyte with the exception of an open window for electrodeposition (ϕ6.0 mm), as shown in Fig. 2(A). Therefore, the exposed area for electrodeposition was 28.3 mm^2. The open circuit potential of titanium, E_{open}, vs. a saturated calomel electrode, SCE, before electrodeposition was measured as *ca.* −0.5 V. Thereafter, the cathodic potential was charged from E_{open} to −5 V vs. SCE with a sweep rate of 0.1 V s^{-1} and maintained at this potential for 300 s. During charging, the terminated PEGs migrated electrically to a titanium cathode, where they were deposited as shown in Fig. 2(B). After electrodeposition, specimens were rinsed in deionized water and dried with a stream of nitrogen gas (99.9%). For comparison, titanium was immersed in an solution containing PEG terminated at both terminals for 24 h without any electric charge.

2.2 Ellipsometry

The thickness of the PEG layer deposited on titanium was determined with an ellipsometer (DVA-36Ls, Mizojiri Optical Co., Ltd.) in air. The use of an ellipsometer resulted in the underestimation of the thickness compared to that in solution. The light source was a He-Ne laser with a wavelength of 632.8 nm, and the incident angle to the titanium surface was 70°. The thickness was calculated by optical constants: the refractive index and absorption coefficient of titanium oxide with the titanium substrate were 2.209 and 3.079,[3,4] and those of the titanium substrate were 2.22 and 2.99,[5] respectively.

Table 1 Photoionization cross sections of level j of element i relative to that of the O 1s, σ_{ij}/σ_{O1s}.

Photoionization cross section			
Level	Ti $2p_{3/2}$	C 1s	N 1s
σ_{ij}	1.28	0.34	0.62
Reference	6	7	7

2.3 XPS

The immobilization manner of PEG to a titanium surface and the chemical bonding state were characterized using XPS (SSX100, SSI, UK). All binding energies given in this paper are relative to the Fermi level, and all spectra were excited with the monochromatized Al Kα line (1486.61 eV). The spectrometer was calibrated against Au $4f_{7/2}$ (binding energy, 84.07 eV) and Au $4f_{5/2}$ (87.74 eV) of pure gold and Cu $2p_{3/2}$ (932.53 eV), Cu $2p_{1/2}$ (952.35 eV), and Cu Auger $L_3M_{4,5}M_{4,5}$ line (kinetic energy, 918.65 eV) of pure copper. The energy values were based on published data.[6] In order to estimate the photoelectron peak intensities, the background was subtracted from the measured spectrum according to Shirley's method.[7] The composition and thickness of the surface oxide and the composition of the substrate were simultaneously calculated according to previous studies.[8,9] Empirical data[10] and theoretically calculated data[11] of the relative photoionization cross sections were used for the quantification. The relative photoionization cross sections used in this study are summarized in Table 1, where σ_{ij}/σ_{O1s} represents the relative photoionization cross section of a level j electron of an element i to that of O 1s electrons.

An angle-resolved technique for XPS was applied to specimens at photoelectron take-off angles of 12°, 24°, 35°, 53°, and 90°, where the take-off angle is defined as the angle between the direction of the photoelectron path to the electron spectrometer and the specimen surface.

2.4 GD-OES

The depth profiles of elements from a PEG-electrodeposited layer and titanium substrate were determined using a GD-OES instrument (Jovin Yvon RF 5000GD-OES, HORIBA, Japan) with a power of 40 W in 600-Pa argon atmosphere. The spectral wavelengths (nm) employed for detecting various elements were as follows: H, 121.57; C, 156.14; N, 149.26; Ti, 365.35; and O, 130.00.[12,13] The sputtering time was converted directly to the depth, assuming that the sputtering rate was constant throughout the analysis of the PEG-electrodeposited layer and titanium substrate.

Table 2 Thicknesses of the PEG layers determined by ellipsometry. B-PEG: PEG terminated at both terminals. O-PEG: PEG terminated at one terminal.

The type of PEG/ immobilization methods	Thickness of PEG layers [nm]
B-PEG/Electrodeposition	2.37
O-PEG/Electrodeoposition	1.85
B-PEG/Immresion	3.87

Mean (standard deviation)

3. Results and Discussion

3.1 Thickness of PEG layers by ellipsometry

Table 2 shows the thicknesses of the PEG deposition layers determined by ellipsometry. These thicknesses are measured in air; therefore, the real thickness in solutions is larger than these values. The thickness of the deposition layer, in other words, the amount of deposited PEG, is the largest in this order: B-PEG immobilized with immersion for 24 h, B-PEG immobilized with electrodeposition for 300 s, O-PEG immobilized with electrodeposition for 300 s (B-PEG: PEG terminated at both terminals. O-PEG: PEG terminated at one terminal). This indicated that electrodeposition was more effective than immersion for the deposition of PEG on the titanium surface.

3.2 Chemical state of titanium and oxygen by XPS

Carbon, oxygen, titanium, and nitrogen were detected using XPS. Sodium and chlorine were not detected. Carbon and nitrogen originate from PEG molecules.

The typical Ti 2p electron energy region peak on the XPS spectrum is shown in Fig. 3. The Ti 2p peak gave four doublets according to the valences, Ti^0, Ti^{2+}, Ti^{3+}, and Ti^{4+}. Published data[14] were used for the binding energy of titanium at each valence. Figure 3 shows an example of the decomposition of the Ti 2p spectrum. Ti^0 originating from a titanium substrate was detected at a large take-off angle but not at a small take-off angle. Ti^{2+}, Ti^{3+}, and Ti^{4+} peaks were detected at all take-off angles and originated from titanium oxide, and the integrated intensity of Ti^{4+} was the largest. The titanium surface oxide mainly consisted of TiO_2 containing a small amount of TiO and Ti_2O_3. In other words, the titanium surface was covered mainly by TiO_2.[15] Therefore, the oxygen detected by XPS originated from PEG molecules and titanium oxide covering the titanium substrate, and titanium originated from both titanium oxide and the titanium substrate.

The O 1s electron energy region peak is deconvoluted to peaks originated from O^{2-}, hydroxide, or hydroxyl groups, OH^-, and hydrate and/or adsorbed water.[16] Naturally, a titanium surface oxide contains hydroxyl groups at the surface and inside the oxide.

3.3 Depth profiles of elements obtained by the XPS angular-resolved technique

The entire PEG layer was detected by XPS because PEG was immobilized on titanium that was covered with titanium oxide. Surface oxide was detected by XPS at all take-off angles, and the titanium substrate was detected only at high take-off angles. When the PEG layer and/or titanium oxide layer is thick, the intensity of Ti^0 decreases because the signal from the titanium substrate is small.

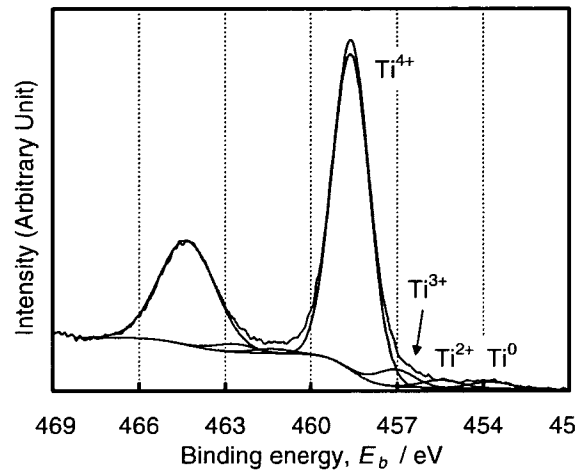

Fig. 3 Typical Ti 2p energy electron region XPS peak and decomposition into eight peaks ($2p_{3/2}$ and $2p_{1/2}$ electron peaks in four valences). The numbers with arrows are valence numbers.

The relative concentrations of carbon, oxygen, titanium, and nitrogen were calculated assuming that the gross amount of these elements, as detected using XPS, was 100 mole percent. The apparent concentrations of elements calculated under the assumption of a homogeneous depth distribution within the PEG-immobilized layer were dependent on the take-off angle, generally suggesting the existence of concentration gradients. The concentrations of carbon, oxygen, titanium, and nitrogen obtained by the angle-resolved technique are plotted in Fig. 4 against the average escape depth of photoelectrons. In the average effective escape depth of photoelectrons for angle-resolved XPS measurements, λ is the average mean-free-path of C 1s, O 1s, Ti 2p, and N 1s photoelectrons, and the effective escape depth is estimated as λ times sin (take-off angle).

The concentrations of carbon at small take-off angles were high, indicating that carbon atoms distribute more in the outer layer than in the inner layer in the PEG layer (Fig. 4(A)). The concentrations of oxygen at small take-off angles were low, indicating that oxygen distributes more in the inner layer than in the outer layer in the PEG/titanium oxide combination layer (Fig. 4(B)). The concentrations of titanium at small take-off angles were low, indicating that titanium distributes more in the inner layer than in the outer layer, which is natural because the PEG layer is formed on titanium oxide covering a titanium substrate (Fig. 4(C)). In these elements, no difference between electrodeposition and immersion was observed.

The concentration of nitrogen is relatively low when compared with those of carbon, oxygen, and titanium (Fig. 4(D)) because the concentration of nitrogen in the PEG molecule is very small (see Fig. 1). At all take-off angles, nitrogen in electrodeposited PEG terminated at both terminals and PEG terminated at one terminal were much smaller than both-terminated deposited with immersion. Nitrogen originates from terminal amines in PEG. The

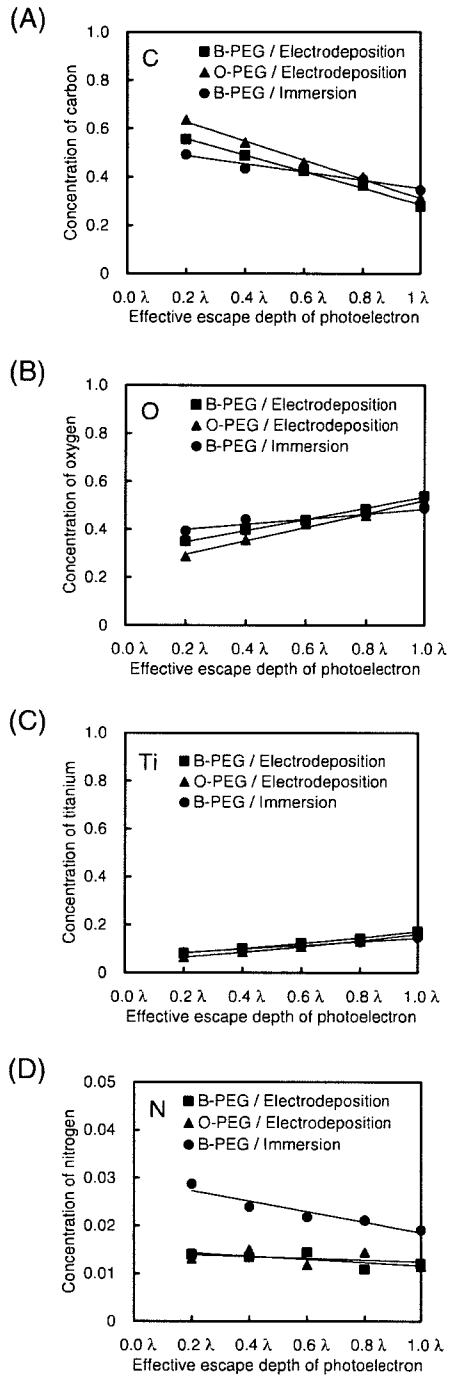

Fig. 4 Concentrations of carbon (A), oxygen (B), titanium (C), and nitrogen (D) against the average effective escape depth of photoelectrons for angle-resolved XPS measurements. Lambda (λ) is the average escape depth of C 1s, O 1s, Ti $2p_{3/2}$, and N 1s photoelectrons, and the effective escape depth is the escape depth times sin (take-off angle). B-PEG: PEG terminated at both terminals. O-PEG: PEG terminated at one terminal.

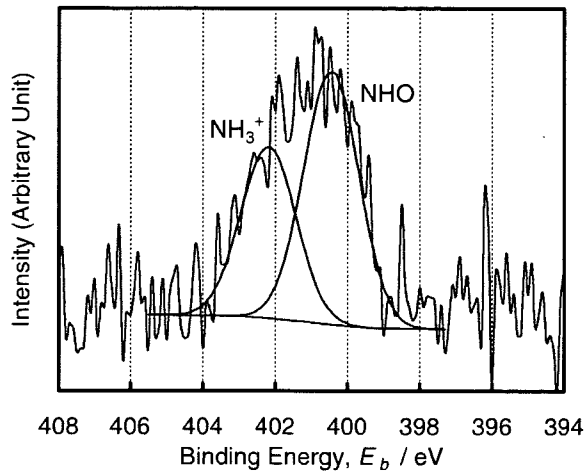

Fig. 5 N 1s electron energy region XPS peak and decomposition of the peak into two component peaks originating from the chemical state of NH_3^+ and NH-O.

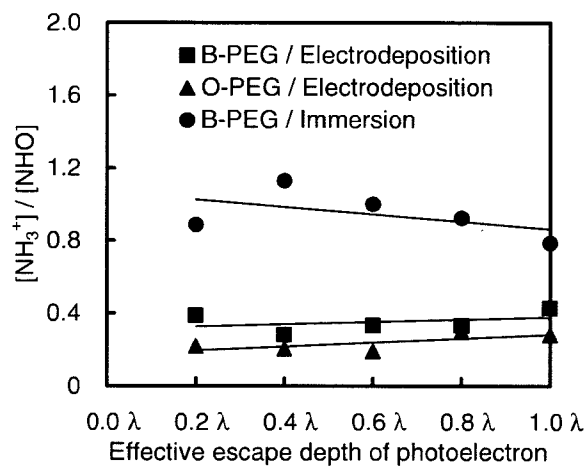

Fig. 6 Ratio of the integrated intensity of a peak originating from NH_3^+ to that from N-HO, $[NH_3^+]/[N\text{-}HO]$, against the average effective escape depth of photoelectrons for angle-resolved XPS measurements. Lambda (λ) is the average escape depth of N 1s photoelectrons, and the effective escape depth is the escape depth times sin (take-off angle). B-PEG: PEG terminated at both terminals. O-PEG: PEG terminated at one terminal.

photoelectron signals detected by XPS from a deep site are weak because they decay as they pass through molecules and solids. Therefore, more nitrogen existed inside the PEG-immobilized layer. The results above show that the PEG layer exists on the titanium surface oxide and the oxide exists on the titanium substrate. In addition, more nitrogen atoms in PEG molecules are located inside the PEG-immobilized layer as a result of electrodeposition than they are with immersion. PEG immobilized on titanium does not always form a single layer; but it forms a multi-layer. Even in this case, nitrogen in each PEG layer exists inside the layer.

3.4 Chemical bonding of amine to a titanium surface as determined by XPS

Typical XPS spectra of an N 1s electron energy region and the deconvolutions of these peaks are shown in Fig. 5 according to published data.[17,18] A change in the ratios, $[NH_3^+]/[N\text{-}HO]$, in the N 1s peak is shown in Fig. 6. This ratio is much smaller in electrodeposited specimens than it is in immersed specimens. Nitrogen atoms in electrodeposited specimens existed as a N-HO bond rather than as NH_3^+. The N-HO bond is preferential at the interface between an amine and a titanium surface, *i.e.*, in the first layer of PEG

deposited, according to the chemical structure of PEG. The NH_3^+ bond is preferential in the second and third layers. The N-HO bond is an ionic bond formed between NH_3^+ and OH^- on titanium oxide. This indicated that a strong ionic bond was formed between the amine and titanium oxide with electrodeposition, while a weaker bond was formed with immersion.

A certain amount of PEG is immobilized on titanium not only with electrodeposition but also with immersion when PEG is terminated by amine and charged in an aqueous solution. However, more terminated amines exist at the surface of titanium and combine with titanium surface oxide as a N-HO bond with electrodeposition, while more amines randomly exist in the PEG layer and fewer amines form an ionic bond with titanium oxide with immersion. In PEG terminated at both terminals, the PEG deposited in a U-shape because both terminals combined with the titanium surface; in PEG terminated at one terminal, the PEG deposited as a brush because only one terminal combined with the surface in the first immobilized layer.

3.5 Depth profiles of elements by GD-OES

The GD-OES results are expressed with the emission lines plotted against the acquisition time. The depth profiles of elements of a PEG layer immobilized with electrodeposition on titanium and that with immersion obtained with GD-OES are shown in Fig. 7. The dashed line represents the interface between the PEG layer and titanium surface oxide, which is determined by the following element profiles: the minimum value in hydrogen and change in the slope of titanium. Hydrogen is absorbed to titanium by a specimen preparation process that includes polishing and electrodeposition. Hydrogen evolution during electrodeposition increases with a cathodic potential according to the Pourvaix diagram;[19] therefore, the amount of absorbed hydrogen increased after electrodeposition.

The nitrogen signal outside the interface originates from PEG molecules, while that inside originates from the nitrogen-absorbed titanium oxide and substrate. In the electrodeposition of PEG terminated at both terminals, nitrogen in the PEG molecules increased toward the interface (Fig. 7(A)); however, in immersion, it decreased (Fig. 7(B)). That is, more nitrogen atoms in PEG molecules are located inside the PEG-immobilized layer formed with electrodeposition than inside that formed with immersion. In this sense, the XPS result shown in Fig. 4(D) is completely in accordance with this GD-OES result.

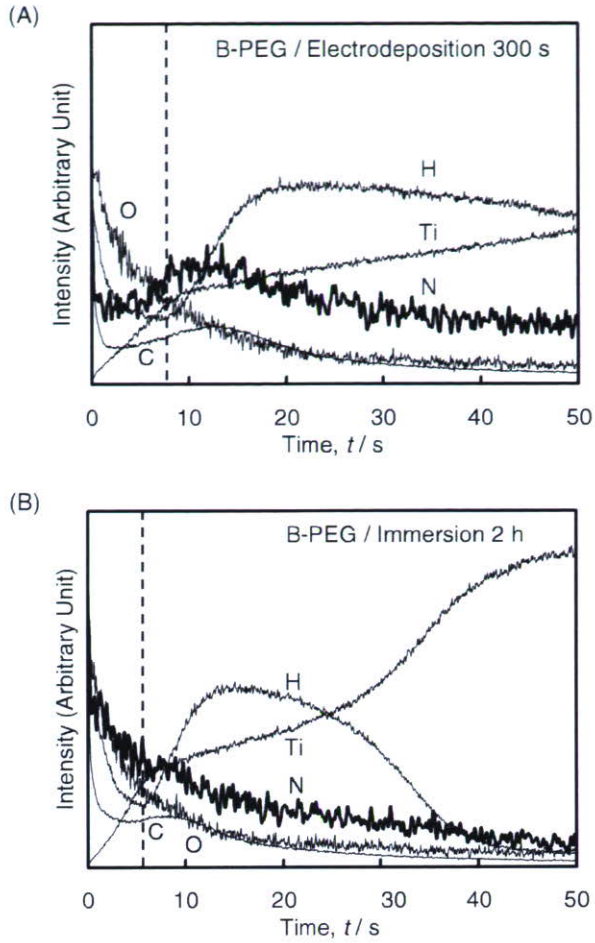

Fig. 7 Depth profiles of elements from PEG-immobilized titanium with electrodeposition (A) and immersion (B) determined by GD-OES. The dashed lines represent the interface between the PEG molecule and titanium.

According to the results above, the immobilization manner of the first PEG layer determined with XPS and GD-OES is illustrated in Fig. 8.

4. Conclusions

In this study, the immobilization manner of PEG terminated with amines at both terminals and at one terminal was characterized with an XPS angular-resolved technique and

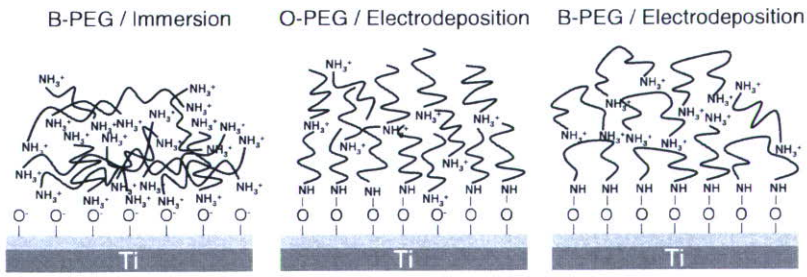

Fig. 8 Schematic model of the deposition manner and chemical bonding state of PEG with immersion and electrodeposition. B-PEG: PEG terminated at both terminals. O-PEG: PEG terminated at one terminal.

GD-OES. In the first layer of immobilized PEG formed with electrodeposition, more terminated amines exist at the interface between the PEG layer and titanium oxide and combine with titanium oxide as a N-HO ionic bond formed between NH_3^+ and OH^-, while more amines randomly exist as NH_3^+ in the PEG layer formed with immersion. In the PEG terminated at both terminals, the PEG immobilized as a U-shape because both terminals combine with the titanium surface; in the PEG terminated at one terminal, the PEG was immobilized as a brush because only one terminal combines with the surface. Over second layers, nitrogen atoms mainly exist as NH_3^+, while nitrogen is located deeper within the PEG layer. The characterization with XPS and GD-OES is useful to determine the immobilization mode of PEG relative to a solid surface.

REFERENCES

1) S. J. Xiao, M. Textor, N. D. Spencer and H. Sigrist: Langmuir. **14** (1998) 5507.
2) Y. Tanaka, H. Doi, Y. Iwasaki, S. Hiromoto, T. Yoneyama, K. Asami, H. Imai and T. Hanawa: Mater. Sci. Eng. C. (in press).
3) *CRC Handbook of Chemistry and Physics*, 67th ed., (CRC Press, Boca Raton, Florida, 1986) pp. E-389–E-390.
4) *Handbook of Optical Constants of Solids*, E. D. Palik ed., (Academic Press, 1985) pp. 233–249.
5) *Handbook of Optical Constants of Solids*, E. D. Palik ed., (Academic Press, 1985) pp. 795–804.
6) K. Asami: J. Electron. Spectrosc. **9** (1976) 469.
7) D. A. Shirley: Phys. Rev. **5** (1972) 4709.
8) K. Asami, K. Hashimoto and S. Shimodaira: Corros. Sci. **17** (1977) 713.
9) K. Asami and K. Hashimoto: Corros. Sci. **24** (1984) 83.
10) K. Asami, S. C. Chen, H. Habazaki, A. Kawashima and K. Hashimoto: Corros. Sci. **31** (1990) 727.
11) J. H. Scofield: J. Electron. Spectrosc. **8** (1976) 129.
12) K. Shimizu, H. Habazaki, P. Skeldon, G. E. Thompson and G. C. Wood: Surf. Interface Anal. **29** (2000) 151.
13) P. L. Coustumer, M. Motelica-Heino, P. Chapon, H. F. Saint-Cyr and R. Payling: Surf. Interface Anal. **35** (2003) 623.
14) K. Asami, S. C. Chen, H. Habazaki and K. Hashimoto: Corros. Sci. **35** (1993) 43.
15) E. J. Kelly: Mod. Aspect. Electrochem. **14** (1982) 319.
16) K. Asami and K. Hashimoto: Corros. Sci. **17** (1977) 559.
17) SR. Sousa, P. Moradas-Ferreira and MA. Barbosa: J. Mater. Sci.: Mat. Med. **16** (2005) 1173.
18) I. Losito, C. Malitesta, I. D. Bari and C. D. Calvano: Thin Solid Films **473** (2005) 104.
19) M. Pourbaix: *Atlas of Electrochemical Equilibria in Aqueous Solution*, (National Association of Chemical Engineers, Houston, TX. 1974).

Materials Transactions, Vol. 48, No. 3 (2007) pp. 301 to 306
Special Issue on Smart and Harmonic Biomaterials

Inhibition Effect of Zirconium Coating on Calcium Phosphate Precipitation of Titanium to Avoid Assimilation with Bone

Equo Kobayashi[1], Miyuki Ando[1,*], Yusuke Tsutsumi[1], Hisashi Doi[1], Takayuki Yoneyama[1], Masahiro Kobayashi[2] and Takao Hanawa[1]

[1]*Institute of Biomaterials and Bioengineering, Tokyo Medical and Dental University, Tokyo 101-0062, Japan*
[2]*Department of Life and Environment Sciences, Chiba Institute of Technology, Narashino 275-0016, Japan*

In order to control of the calcium phosphate precipitation of Ti in body fluid, which might result in assimilated bone re-facture during removal operation of implanted devices such as femoral nails and bone screws after healing, vacuum vapor deposition of Zr on Ti Substrate was carried out. The calcium phosphate precipitation was evaluated through the immersion test into the Hanks' solution. Scanning electron microscopy (SEM) and X-ray photoelectron spectroscopy (XPS) were conducted to evaluate inhibition effect of coated Zr layer.

Calcium phosphate particle were observed on the Ti with and without 90-nm thick Zr coated layer by SEM. On the other hand, on the specimens with 130-nm thick Zr coated layer and those of Zr sputter-coated, no calcium phosphate particle was observed. By the surface analysis of the specimens Zr sputter-coated, Ca was not identified. It was considered to form zirconium phosphate instead of calcium phosphate by immersion in the Hanks' solution. It was suggested that Zr coating technique can be applied to orthopedic devices to avoid re-fracture of bone by calcium phosphate precipitation during removal operation. [doi:10.2320/matertrans.48.301]

(Received September 27, 2006; Accepted December 18, 2006; Published February 25, 2007)

Keywords: *biomedical titanium alloys, zirconium coating, surface modification, calcium phosphate, biocompatibility*

1. Introduction

Due to its less toxicity and superior biocompatibility, Ti and its alloys are used as biomaterials widely in the field of orthopedics. It is well known that Ti is thermodynamically active against to maintain a stable passive oxide film. This passive film acts as a protective film for corrosion. In a macroscopic view, the film is stable, namely inactive. However the partial dissolution and precipitation are repeated constantly in a microscopic view.[1)] Therefore, when Ti is implanted in living body, the composition of the oxide film is gradually changed by influence of the environment during repeated dissolution and precipitation. Elements contained in body fluid, such as P, Ca and S are involved in oxide film. Then calcium phosphate is formed on the surface of Ti. This phenomenon is confirmed both *in vivo* and *in vitro*.[2–4)] In general, bone conductivity of a material could be evaluated with the formation of calcium phosphate on the material in a simulated body fluid.

For the fast fixation of artificial hip joints to hard tissue after surgical operation, the enhancement of this calcium phosphate precipitation is a key technology and several kinds of surface modification have been developed, such as electrolysis techniques,[5,6)] immersion in alkaline solution,[7)] immersion in hydrogen peroxide,[8)] hydro-thermal treatment[9)] and calcium ion implantation[10,11)] to modify the surface inducing active interactions between the modified surface and hard tissue. Some of them have been already applied to the commercial artificial hip joints to shorten the fixation period.

However, for some kinds of internal fixation devices implanted into marrow, such as femoral, tibial and humeral nails and screws for bone plate fixation, titanium's property forming fastly calcium phosphate is not ideal. For these removal implant devices, assimilation with bone by the calcium phosphate precipitation might cause in re-fracture of the bone during removal operation. Thus, for the removal implant devices into marrow, the inhibition of the calcium phosphate precipitation is required. The requirement is completely opposite against the purpose of a large portion of surface treatments in Ti materials for the acceleration of bone formation.

Zirconium is known to have less toxicity and good corrosion resistance similar to Ti. Ti-13Nb-13Zr alloy has been developed in early 1990s as a beta-type Ti orthopedic alloy. In the previous paper on alloys' surface analysis after immersion into Hanks' solution, an artificial body fluid simulating inorganic components of the extracellular body fluid, zirconium phosphate precipitation was observed on pure Zr and Ti-Zr binary alloys containing more than 34.4 mol%[3)] instead of calcium phosphate precipitation seen, while calcium phosphate was precipitated on Ti and Ti-14.9 mol%Zr alloy. It was concluded that zirconium oxide didn't involve Ca ion during repeated dissolution and precipitation of oxide. In other words, Zr has an ability to prevent the precipitation of calcium phosphate.

In the present study, vacuum vapor deposition of Zr onto the Ti disk substrates was carried out in order to control of the calcium phosphate precipitation of Ti. The calcium phosphate precipitation was evaluated through the immersion test into the Hanks' solution, followed by scanning electron microscopy, SEM, and X-ray photoelectron spectroscopy, XPS.

2. Experimental

2.1 Specimens

Disks of Ti (10 mm in diameter and 1.5 mm in thickness) were cut out from pure Ti rods (99.9 mass% in purity, Nilaco) by an abrasive wheel cutter. Top surface for Zr deposition was mirror-polished with diamond paste (9 μm) and alumina

*Undergraduate Student, Chiba Institute of Technology. Present address: Sankosha Engineering, 988 Kanoyamachi, Hachioji 192-0815, Japan

Table 1 Ion concentration of Hanks' solution.

Ion	Na^+	K^+	Mg^+	Ca^+	Cl^-	HCO_3^-	HPO_4^{2-}	SO_4^{2-}
Concentration (mol%)	141.9	5.8	1.7	1.3	144.8	4.2	0.9	1.7

paste (0.05 μm). Bottom surface and round surfaces were finished with 320 grid SiC papers.

Vacuum vapor deposition of Zr onto the Ti disk substrates was carried out using a commercial vacuum evaporator (JEE-420, JEOL) with Zr ingots on tungsten baskets. The basket (Zr ingot) height was fixed 80.0 mm above of the Ti disks. Five or six disks were deposited same time of deposition. Zirconium ingots were made from sponge Zr (99.6 mass% in purity, Toho Titanium) by argon arc melting on a water-chilled cupper hearth. Half-masked disks were used to measure Zr coated layer thickness. Coated layer thickness was measured using a laser profile microscope (VF-7500, Keyence) by step height of coated part and uncoated part of a specimen which was half-masked tightly with a small piece of thin paper.

Reference materials, such as Ti without Zr and sputter-coated Zr on Ti substrates (Hokuto Denko) were also tested. The thickness of the coated layer on the latter specimens was approximately 1 μm which was measured by the cross-sectional optical microscopy of a specimen. The surface of sputter-coated Zr showed slight roughness ($R_a = 0.26$ μm).

2.2 Immersion test in Hanks' solution

The immersion test was conducted with Hanks' solution (pH 7.4), an artificial body fluid simulating inorganic components of the extracellular body fluid, at 310 K. The ion contents of Hanks' solution are shown in Table 1. Specimens were immersed into 50 mL of Hanks' solution in sealed containers made of polytetrafluoroethylene (PTFE) for 1 d (specimens for XPS) or 7 d (those for SEM). The PTFE containers were kept in an incubator to keep the temperature at 310 K. For the immersion test for SEM, Hanks' solution was changed once in three days. The pH alteration during immersion tests was detected using a pH meter (HM-60V, DKK-Toa).

2.3 Surface observation and analysis

Surface observation was carried out with specimens after immersion test for 7 d with an SEM (JSM-6400, JEOL) at 7 to 15 kV of acceleration voltage. Surface analysis for 1 d immersed specimens was conducted with an XPS (SSX-100, SSI). An X-ray source was monochromatized Al Kα (1486.61 eV) accelerated with 15 kV. The photoelectrons were detected through 58.7 eV in FAT pass energy, with 35° of detection angle under a vacuum atmosphere at 10^{-7} Pa or less. Binding energies of photoelectrons were calibrated by binding energy peak of C 1s (binding energy, 285.0 eV) originating from so-called contaminated carbon. The spectrometer was calibrated against Au $4f_{7/2}$ (84.07 eV) and Au $4f_{5/2}$ (87.74 eV) of pure gold and Cu $2p_{3/2}$ (932.53 eV), Cu $2p_{1/2}$ (952.35 eV) and Cu Auger $L_3M_{4,5}M_{4,5}$ line (kinetic energy, 918.65 eV) of pure cupper. The energy values were based on the published data.[12] Analysis was conducted at least two points of a specimen. The composition and thickness were determined with an inductively calculating method presented by Asami *et al.*[13]

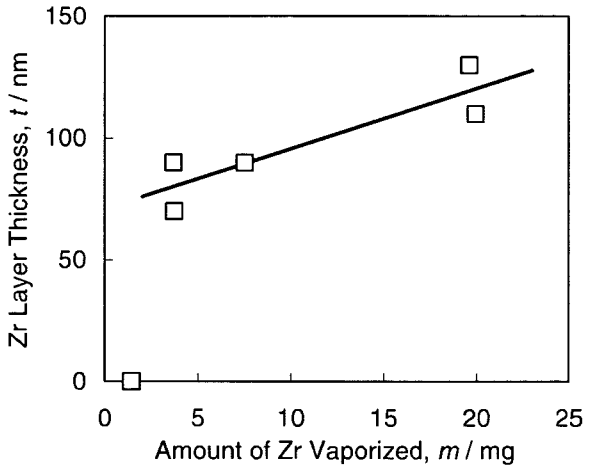

Fig. 1 Relation between amount of Zr vaporized and layer thickness after vapor deposition.

3. Results and Discussion

3.1 Thickness of Zr coated layer

Mass loss of Zr ingot after each vacuum vapor deposition was varied from 3.69 mg to 19.95 mg. Relation between mass loss and thickness of Zr coated layer measured by the laser profile microscope is shown in Fig. 1. It shows good liner relation at higher than 3.69 mg vapor deposition. It is suggested that the thickness of Zr coated layer can be controlled by the vaporized amount of Zr.

3.2 SEM observation after immersion test

Scanning electron micrographs of surface of Ti without Zr coating, Ti with Zr vapor deposited with coating thickness as 90 nm and 130 nm, and Ti with Zr sputter-coated are shown in Fig. 2. On the surface of Ti without Zr coating, precipitates with 1 μm in diameter are observed. In contrast, no precipitates were observed on Ti specimens with Zr vapor-coated layer. On the specimen with sputter-coated layer showed very small amount of precipitates. It is considered formed on the sputter-coated layer due to its rough surface.

3.3 XPS surface analysis before and after immersion test

Specimens immersed into the Hanks' solution for 1 d were used for the XPS analysis. Figure 3 shows the survey spectrum of the specimens (a) before and (b) after immersion. From the Ti without and with Zr vapor deposited (90 nm thickness) after immersion into Hanks' solution, peaks corresponding to binding energy of P 2p clearly seen.

Figure 4 shows narrow area spectrum of P, Ca, Ti, Zr and O. Examples of peak of P, Ca, Ti and O are taken from Ti without Zr coating after 1-d immersion in the Hanks' solution, while that of Zr from Ti with Zr vapor deposited with 130-nm coating thickness.

Spectra of P 2p was obtained as combined peak at around 134 eV. According to the previous report, P 2p binding

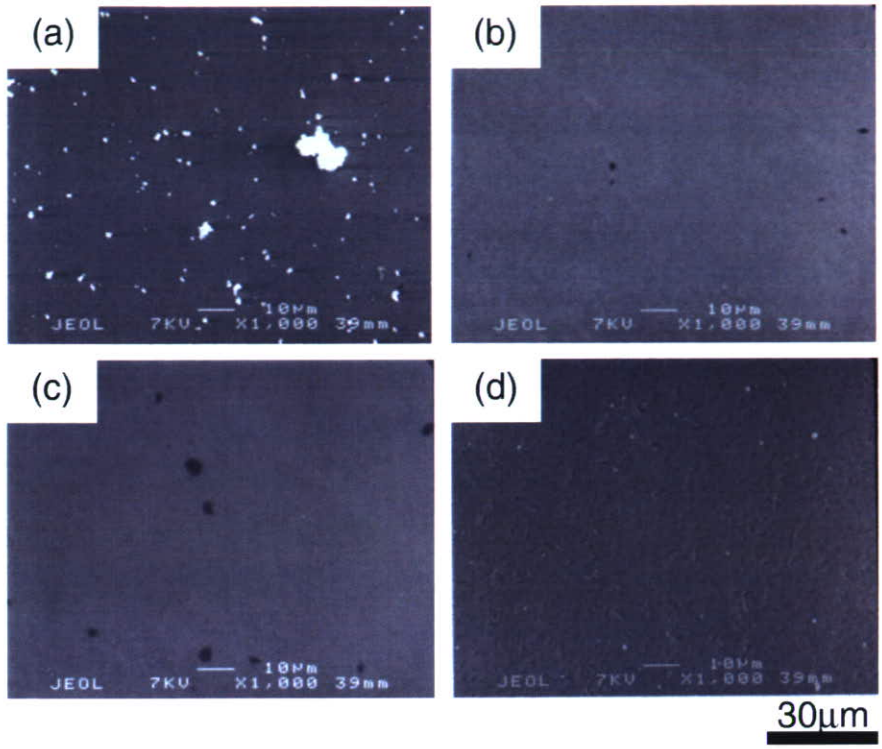

Fig. 2 Specimens' surface after 7 d immersion into Hanks' solution at 310 K, (a) Ti without Zr coating, (b) Ti with Zr vapor-coated (90 nm), (c) Ti with Zr vapor-coated (130 nm), and (d) Ti with Zr Spatter-coated.

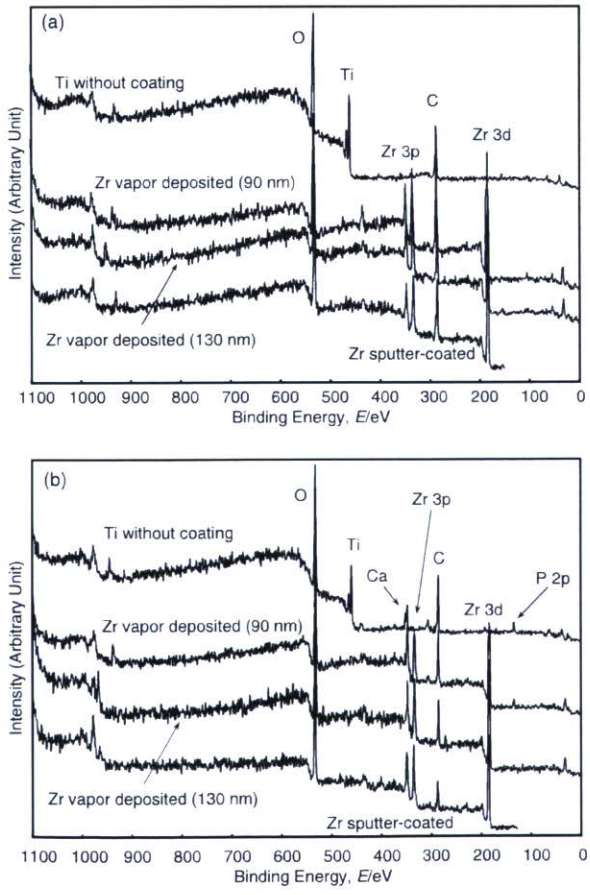

Fig. 3 Survey spectrum of specimens, (a) before and (b) after immersion into Hanks' solution for 1 d.

energies of potassium phosphates and sodium phosphates are varied from 132.7 eV to 133.9 eV, while those of several calcium phosphates, such as $Ca_{10}(PO_4)(OH)_2$, $CaHPO_4 \cdot H_2O$ and $Ca(H_2PO_4)_2 \cdot H_2O$ are 133.2 eV to 134.3 eV.[2] Although it was difficult to deconvolute the spectra of P 2p into $H_2PO_4^-$, HPO_4^{2-} and/or PO_4^{3-} in the present study, the combined peak around 134 eV shows good correspondence to P 2p binding energies of calcium phosphates in the previous report. Doublet peaks of Ca 2p was identified as Ca $2p_{1/2}$ and Ca $2p_{3/2}$ referring to previous report.[2,3]

The peak of Ti was deconvoluted into Ti^0 from metallic substrate and cations having different valence (Ti^{2+}, Ti^{3+}, Ti^{4+}). On the other hand, only tetra-valent oxide was detected for Zr in the present study. According to previous report, peak from O 1s can be deconvoluted into O^{2-}, OH^- and H_2O.[13] They correspond to binding energy of hydroxyl, bound water or adsorbed water in the oxide layer and oxygen consisting oxide, respectively. Because phosphate groups were detected in Ti without Zr coating specimen together with only cation Ca^{2+}, the particles seen in SEM observation were concluded as calcium phosphates.

Quantitative analysis based on the peak deconvolution shown in Fig. 4 was carried out. Concentration of P and Ca taken from specimen after 1-d immersion in Hanks' solution is shown in Fig. 5. In the Ti without Zr coating and the 90-nm thick Zr deposited specimen, approximately 3 mol% of P and Ca was detected, while 1.5 mol% of P and no Ca was exist on the specimen the 90 nm thick Zr deposited and that Zr sputter-coated. It is considered that this difference was presumably caused from imperfection of coated layer.

The ratio, [Ca]/[P], on the Ti without Zr specimen,

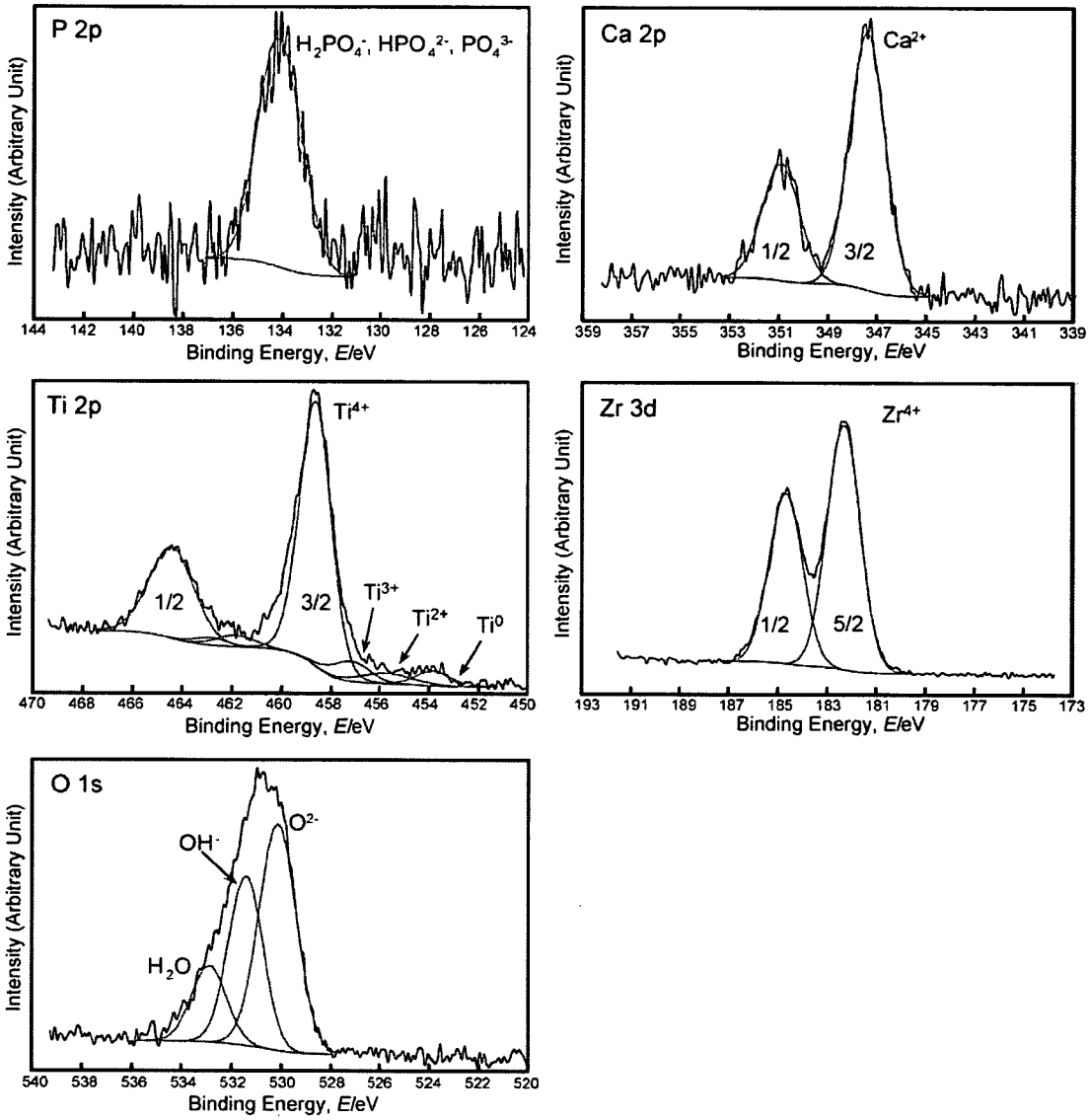

Fig. 4 Examples of peak deconvolution of narrow area spectrum of XPS analysis for P, Ca, Ti, Zr and O. All of the example spectrum are taken from specimen of Ti without Zr coating after immersion, except Zr spectra which is taken from that of Ti with Zr vapor deposited with 130-nm coating thickness.

calculated from above results was about 1.2. It is slightly smaller than that of hydroxyapatite ($Ca_{10}(PO_4)_6(OH)_2$), which is known to 1.67, and rather nearer to that of $Ca_8(HPO_4)_2(PO_4)_4$, which is 1.33.[3)]

According to the previous report, zirconium phosphate was observed on the pure Zr (purity > 99.9%) surface instead of calcium phosphate.[14)] It is reported that phosphate ion adhesion was occurred by dehydration and oxidation as follows,

$$\begin{aligned} &Zr(OH)^{3+}{}_{(ox)} + H_2PO_4{}^-{}_{(aq)} \Leftrightarrow Zr^{4+}{}_{(ox)}\cdot HPO_4{}^{2-}{}_{(ads)} + H_2O \\ &Zr^{4+}{}_{(ox)}\cdot HPO_4{}^{2-}{}_{(ads)} + OH^- \Leftrightarrow Zr^{4+}{}_{(ox)}\cdot PO_4{}^{3-}{}_{(ads)} + H_2O \\ &Zr(OH)^{3+}{}_{(ox)} + HPO_4{}^{2-}{}_{(aq)} \Leftrightarrow Zr^{4+}{}_{(ox)}\cdot PO_4{}^{3-}{}_{(ads)} + H_2O \end{aligned} \quad (1)$$

Suffixes of ox, aq and ads correspond to ions in oxide, aqueous solution and adhesion respectively. After these reactions, these phosphate ions were involved in oxide layers as forms of PO_4^{3-}, HPO_4^{2-} and $H_2PO_4^-$. According to the report, on the Ti surface, the adhesion of phosphate ions and Ca ion occurs alternately resulting in calcium phosphate precipitation. On the other hand, on the Zr surface, Ca ion adhesion is obstructed due to an interaction between the oxide and Ca ion, zirconium phosphate can be precipitated. In the present study, spectra of P was observed on the Zr sputter-coated specimens, which are considered to maintain the most fixed Zr layers, no spectra of Ca was detected.

As shown in Fig. 5, approximately 80% of atoms were O in the general results of quantity analysis by XPS. Ratio of the P and Ca is already stated above. N, Na and Si are considered as surface contamination.

According to the results of peak deconvolution of O spectra into O^{2-}, OH^-, and H_2O, which correspond to hydroxyl absorbed on surface oxide, water molecules mainly absorbed on oxide surface, and oxygen in the titanium oxide (TiO_2) and/or zirconium oxide (ZrO_2) respectively, state

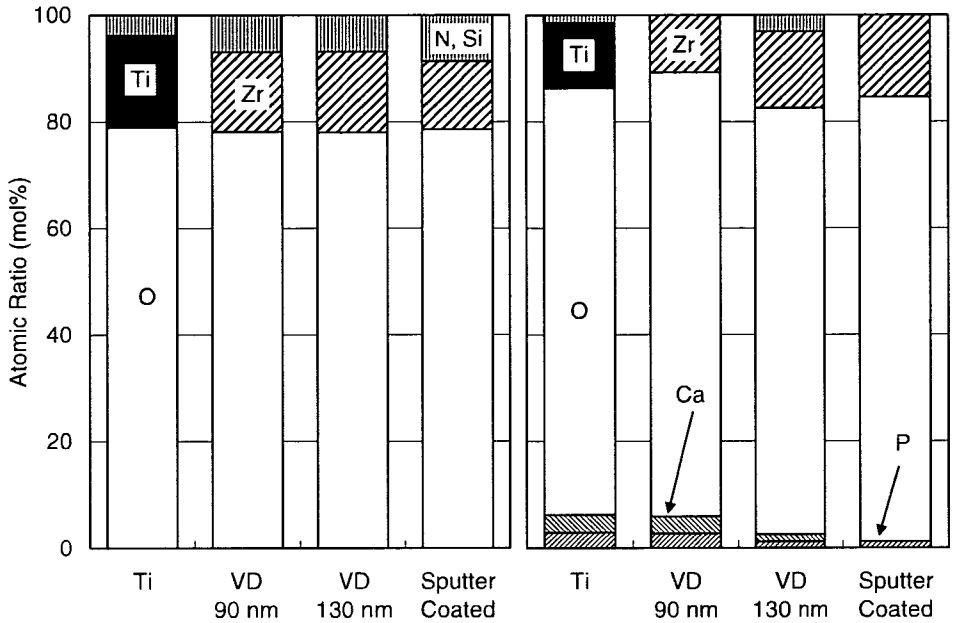

Fig. 5 Atomic ratio of specimens (left) before and (right) after immersion in Hanks' solution for 1 d. Ti: Ti without Zr coating, VD: vapor deposited. N and Si were contamination atoms.

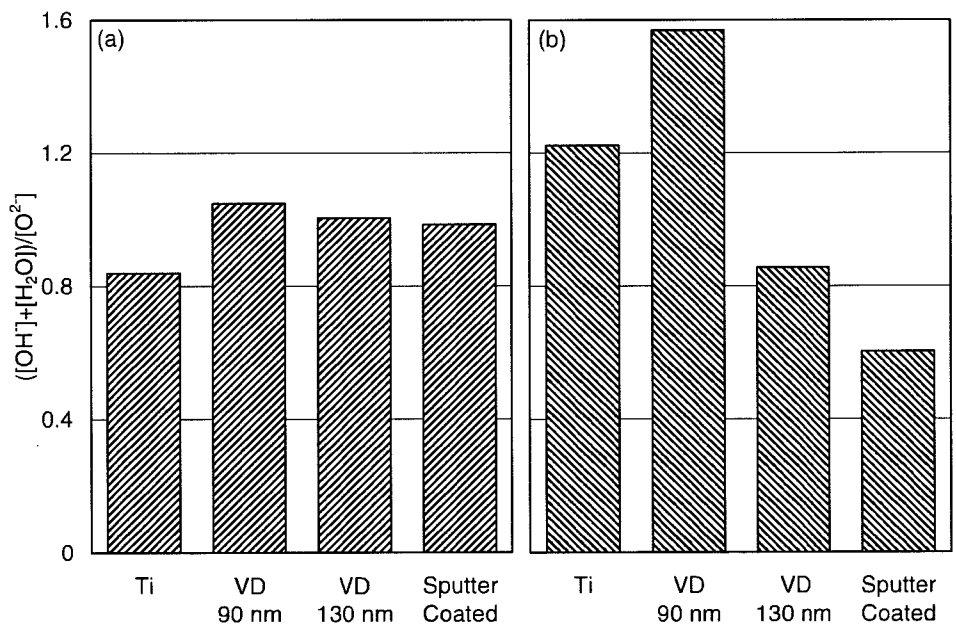

Fig. 6 $([OH^-] + [H_2O])/[O^{2-}]$ ratio of specimens (a) before and (b) after immersion in Hanks' solution for 1 d. Ti: Ti without Zr coating, VD: vapor deposited.

analysis was carried out. Figure 6 indicates ratio of oxygen on the oxides surface (OH^- and H_2O) for that in the oxides (O^{2-}). From the surface analysis before Hanks' solution immersion, the specimens Zr vapor deposited and that Zr sputter-coated showed higher $([OH^-] + [H_2O])/[O^{2-}]$ value than Ti without Zr. Comparing the $([OH^-] + [H_2O])/[O^{2-}]$ value before and after immersion, $([OH^-] + [H_2O])/[O^{2-}]$ value increased for the Ti specimen without Zr and the specimens Zr vapor deposited (90-nm thick), while the value decreased for the specimens Zr vapor deposited (130-nm thick) and Zr sputter-coated.

If once Zr is immersed into aqueous solution, following reactions might occur on the surface.[3)]

$$Zr_2O_3 + 4OH^- \rightarrow 2ZrO(OH)_2 + H_2O + 2e^-$$
$$2ZrO(OH)_2 \rightarrow ZrO_2 + 2H_2O \quad (2)$$

According to these reactions, oxides film grows (which results in increasing of $[O^{2-}]$) and the $([OH^-] + [H_2O])/[O^{2-}]$ value will be decreased. Decreasing in the specimens Zr deposited (130-nm thick) and Zr sputter-coated

can be understood by this description. On the other hand, the $([OH^-] + [H_2O])/[O^{2-}]$ value in the Ti specimen without Zr and the specimen Zr deposited (90-nm thick) was increased after immersion into Hanks' solution. It is considered due to calcium phosphate formation on these specimens. As shown in equations (1), hydroxyl group contributes to reactions for calcium phosphates. In the recent reports, it was also reported that there is a certain relation between quantity of hydroxyl and crystallization of calcium phosphate.[6)]

4. Conclusion

On the surface of Ti without Zr, particle precipitates were observed and they were analyzed as calcium phosphate. Calcium phosphate was also identified on the specimens with 90-nm thick Zr coated layer. On the other hand, the specimens with 130-nm thick Zr coated layer exhibited control of calcium phosphate precipitation on the surface. By the surface analysis of the specimens Zr sputter-coated, Ca was not identified. It was considered to form zirconium phosphate instead of calcium phosphate.

From above results, efficiency of vapor deposited coating of Zr on inhibiting calcium phosphate in the body fluid was confirmed. It will be more effective when the thickness of the coated layer becoming thicker. Within the XPS results in the present study, it was confirmed that the sputter coating which provides thicker layer can prevent calcium phosphate precipitation. It was suggested that this technique can be applied to orthopedic devices such as femoral, tibial and humeral nails and bone screws to avoid re-fracture of bone by calcium phosphate precipitation during removal operation.

REFERENCES

1) E. J. Kelly: Mod. Aspect Electrochem. **14** (1982) 319–424.
2) T. Hanawa and M. Ota: Biomaterials **12** (1991) 767–774.
3) T. Hanawa, O. Okuno and H. Hamanaka: J. Jpn. Inst. Metals. **56** (1992) 1168–1173.
4) M. Fini, A. Cigada, G. Rondelli, R. Chiesa, R. Giardino, G. Giavaresi, N. N. Aldini, P. Torricelli and B. Vicentini: Biomaterials **20** (1999) 1587–1594.
5) S. Ban and S. Maruno: Biomaterials **19** (1998) 1245–1253.
6) Y. Tanaka, E. Kobayashi, S. Hiromoto, K. Asami, H. Imai and T. Hanawa: J. Mater. Sci. Mater. Med. in press.
7) H. M. Kim, F. Miyaji, T. Kokubo and T. Nakamura: J. Biomed. Mater. Res. **32** (1996) 409–417.
8) C. Ohtsuki, H. Iida, S. Hayakawa and A. Osaka: J. Biomed. Mater. Res. **35** (1997) 39–47.
9) K. Hamada, M. Kon, H. Ukai, K. Murakami, Y. Miyamoto and K. Asaoka: Biomaterials **23** (2002) 2265–2272.
10) T. Hanawa, S. Kihara and K. Murakami: *Characterization and Performance of Calcium Phosphate Coatings for Implants*, ed. by E. Horowitz and J. E. Parr, (ASTM, Philadelphia, ASTM STP 1196), pp. 170–184.
11) T. Hanawa, K. Asami and K. Asaoka: Corros. Sci. **38** (1996) 1579–1594.
12) K. Asami: J. Electron Spectrosc. **9** (1976) 469–478.
13) K. Asami, K. Hashimoto and S. Shimodaira: Corros. Sci. **17** (1977) 713–723.
14) T. Hanawa, K. Asami and K. Asaoka: J. Biomed. Mater. Res. **40** (1998) 530–538.

Available online at www.sciencedirect.com
ScienceDirect
Surface & Coatings Technology 201 (2007) 7686–7691
SURFACE & COATINGS TECHNOLOGY
www.elsevier.com/locate/surfcoat

Characterization of calcium titanate thin films deposited on titanium with reactive sputtering and pulsed laser depositions

Naofumi Ohtsu [a,b,*], Akihiko Ito [a], Kesami Saito [a], Takao Hanawa [b]

[a] *Institute for Materials Research, Tohoku University, Sendai 980-8577, Japan*
[b] *Institute of Biomaterials and Bioengineering, Tokyo Medical and Dental University, Tokyo 101-0062, Japan*

Received 24 January 2007; accepted in revised form 27 February 2007
Available online 12 March 2007

Abstract

In the present study, characteristics of calcium titanate thin films deposited on titanium by reactive sputtering and pulsed laser deposition techniques were investigated. In both techniques, a calcium titanate target was used as a deposition source, and the titanium substrate was heated at 873 K during the deposition. The oxygen flow for the reactive sputtering was in the range of 1 to 10 sccm, and the oxygen pressure for the pulsed laser deposition was in the range of 0.13 to 13 Pa. The deposited films were crystallized into perovskite-type calcium titanate; furthermore, a titanium-dioxide layer formed in the interface between the film and substrate. In the film deposited by reactive sputtering with low oxygen flow, titanium-to-calcium ratio ([Ti]/[Ca]) is lower than that of stoichiometric calcium titanate due to the formation of calcium hydroxide. The ratio increases with an increase of oxygen flow, and the ratio of the film deposited with a 10-sccm oxygen flow was almost in accordance with that of stoichiometric calcium titanate. On the other hand, in the pulsed laser deposition, [Ti]/[Ca] ratios of the deposited film were almost in accordance with that of stoichiometric calcium titanate at the oxygen pressure under the present experimental condition. In both deposition techniques, the thickness of the titanium-oxide layer increased with an increase of the amount of oxygen gases. The results indicate that the pulsed laser deposition has an advantage for the preparation of the stoichiometric calcium titanate film without formation of a thick titanium-oxide layer.

Keywords: Film characterization; Calcium titanate film; Reactive sputtering deposition; Pulsed laser deposition

1. Introduction

One of the purposes of surface modifications for biomaterials is to improve tissue responses in a living body because tissue-biomaterial reactions are interfacial phenomena which are governed by surface properties of the biomaterial. Ceramic coatings are often applied to facilitate osteogenesis on metallic biomaterials. Among ceramics, hydroxyapatite (HAP) is the most popular coating material [1–5]. Many researchers have demonstrated good osteogenesis on HAP-coated metals [6–9], and HAP-coated titanium prepared with a plasma-spraying process has been used clinically [10–12]. However, fractures at the HAP-titanium interface and in the HAP layer itself are often observed after long-term use in the human body [13]. Accidents caused by these fractures result in a loss of the biomaterial-bone fixation. Consequently, clinical use of the HAP-coated titanium has decreased in recent years.

Recently, some of the present authors succeeded in developing a bioactive calcium titanate ($CaTiO_3$) film which can activate osteogenesis on titanium [14–17]. The bioactive $CaTiO_3$ film was prepared by radiofrequency (RF) magnetron sputtering with a $CaTiO_3$ target in an argon atmosphere and post-annealing at 873 K in air [16,17]. The prepared film was crystallized into perovskite-type $CaTiO_3$, and the chemical composition of the film was almost in accordance with that of stoichiometric $CaTiO_3$. A remarkable feature of the bioactive $CaTiO_3$ film was that the thickness was about 50 nm [17]. The thickness was 1/1000 that of plasma-sprayed HAP coating. This thickness made it possible to improve the mechanical strength

* Corresponding author. Institute for Materials Research, Tohoku University, 2-1-1 Katahira, Aoba-ku, Sendai 980-8577, Japan. Tel.: +81 22 215 2375; fax: +81 22 215 2157.
E-mail address: nohtsu@imr.tohoku.ac.jp (N. Ohtsu).

0257-8972/$ - see front matter © 2007 Elsevier B.V. All rights reserved.
doi:10.1016/j.surfcoat.2007.02.043

of the film itself. However, the post-annealing in air yielded not only crystallization of the $CaTiO_3$ film but also the formation of a titanium-oxide layer in the interface between the film and the titanium substrate because of the oxidation of titanium, resulting in a change in the interface properties.

Some of the authors showed that the adhesion strength of the $CaTiO_3$ film increases with a decrease in the thickness of the interfacial TiO_2 layer [15]. By thinning the TiO_2 layer up to half its thickness, the adhesion strength estimated by the tensile test increased by approximately 40%. Likewise, Kobayashi et al. reported that, in the case of sodium titanate film, the formation of an interfacial TiO_2 layer formed by heating weakened the adhesion strength [18]. Consequently, in order to obtain a non-destructive bioactive $CaTiO_3$ layer, development of new coating process without formation of the thick oxide layer is required.

In the present study, characteristics of $CaTiO_3$ films on titanium deposited both by reactive sputtering and by pulsed laser deposition techniques were investigated. In both techniques, titanium substrates were kept at 873 K to obtain a crystallized $CaTiO_3$ film without post-annealing. Chemical states and atomic concentration of elements of deposited $CaTiO_3$ film were characterized with X-ray photoelectron spectroscopy (XPS), and crystal phase was identified with grazing incident angle X-ray diffractometry (GI-XRD). The thickness of the titanium-oxide layer formed in the interface was evaluated by depth analysis with Auger electron spectroscopy (AES).

2. Experimental procedure

2.1. Deposition of $CaTiO_3$ thin film

Commercial pure titanium (cpTi) with a purity of 99.9% (Furuuchi Chem. Co., Japan) was used as a substrate. The titanium disk (Φ 8 mm × t 1 mm) was mechanically polished with SiC paper (#1000). After polishing, the titanium disk was washed ultrasonically in acetone. The $CaTiO_3$ targets used for reactive sputtering and pulsed laser deposition techniques were prepared by the following sintering method: a commercial regent of $CaTiO_3$ with a purification of 99.9% was compacted into an appropriate dimension for the target by cold press, and the $CaTiO_3$ compact was sintered at 1523 K for 10.8 ks.

In both of the deposition processes, the cpTi substrate was kept at 873 K during the deposition, and the thickness of deposited $CaTiO_3$ films was adjusted to ca. 50 nm by controlling the deposition time. The deposition time was calculated from the deposition rate determined by a stylus-type surface profiler. The deposition rate of reactive sputtering deposition decreased with an increase of the reaction gases, whereas that of the pulsed laser deposition was constant.

For the reactive sputtering deposition, a radiofrequency (RF) magnetron sputtering system with a $CaTiO_3$ target was used [14,15]. The pressure of the deposition chamber just before the deposition (base pressure) was approximately 10^{-7} Pa. High-purity argon and oxygen gases were introduced into the chamber through a mass flow controller as working and reaction gases, respectively. The deposition was carried out in oxygen flows of 1, 3, 5, and 10 sccm. The RF power supply of the target was fixed at 200 W, and the target-to-substrate distance was 250 mm.

For the pulsed laser deposition, a third harmonic wavelength of a Q-switch pulsed Nd:YAG laser (Spectron Laser System SL805, $\lambda = 335$ nm and repetition: 10 Hz) was used for the ablation. The laser beam was introduced into a deposition vacuum chamber through a quartz window and irradiated on the $CaTiO_3$ target at a 45-degree angle to the surface. The target-to-substrate distance was 60 mm. Power density of the laser output was 2×10^4 J m^{-2}. The base pressure of the chamber was approximately 10^{-7} Pa, and the pulsed laser deposition was carried out in oxygen atmospheres at pressures of 0.13, 1.3, and 13 Pa.

2.2. Characterization of the deposited $CaTiO_3$ film

The chemical state and its composition at the film surface were analyzed with XPS. The photoelectrons were excited by Al Kα radiation (hv = 1486.6 eV) from a monochromatized X-ray source (SSX-100, Surface Science Inc., U.S.A). The spot size of the X-ray on the specimen was approximately 300×500 μm^2. The binding energy and FWHM of Au $4f_{7/2}$ were 84.0 and 1.1 eV, respectively. The atomic ratio of titanium to calcium was estimated from the integrated intensities of Ti $2p_{3/2}$ and Ca $2p_{3/2}$, where the sensitivity factors installed in the standard SSI software were used for the calculation. Crystal phase was identified by GI-XRD with a step-scanning mode at 1.3×10^{-2} deg s^{-1} and the X-ray incident angle $\alpha = 1.0°$ against the specimen surface (Rotaflex RU-200B, Rigaku, Japan). Depth profiles of the elements were determined with AES

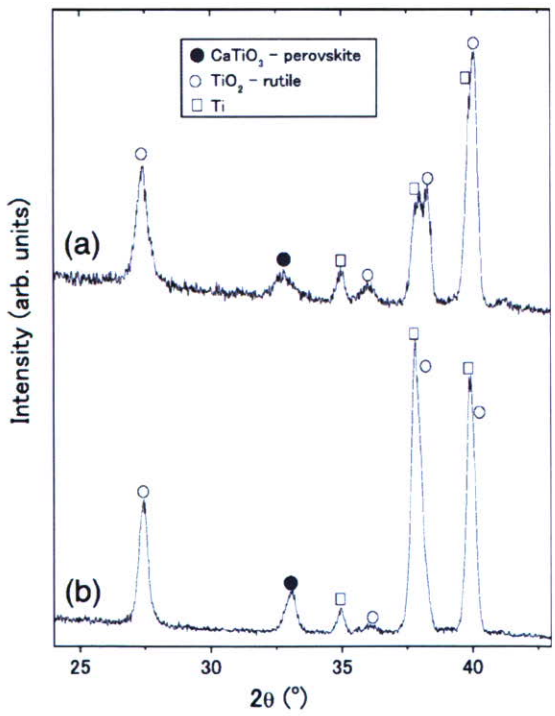

Fig. 1. GI-XRD patterns of $CaTiO_3$ thin film deposited on titanium: (a) by reactive sputtering with a 10-sccm oxygen flow, (b) by pulsed laser deposition in an oxygen atmosphere at a pressure of 1.3 Pa.

(JAMP-7100E, JEOL, Japan) with an argon-ion sputtering system. The acceleration voltage of the electron probe was 10 kV, and that of Ar ions for ion sputtering was 3.0 kV. The sputtering rate was estimated with SiO_2 film on Si substrate. The profiles were determined by monitoring differential spectra for Ti $L_3M_{23}M_{23}$, Ca $L_3M_2M_3$, and O KVV transition lines.

3. Results and discussions

3.1. Characteristics of the deposited $CaTiO_3$ thin films

Typical GI-XRD patterns of the $CaTiO_3$ deposited on the titanium are shown in Fig. 1. Since the effective depth of GI-XRD analysis at $\alpha = 1°$ is larger than the thickness of the film, the GI-XRD patterns include the peaks from the deposited film, interface layers between the film and the titanium substrate, and the titanium substrate. In the both patterns, peaks are assigned to perovskite-type $CaTiO_3$, rutile-type TiO_2, and Ti peaks. The origin of the TiO_2 is the titanium-oxide layer formed in the interface, which is revealed in the AES depth profiles shown later. It is clear that the origins of the $CaTiO_3$ and Ti peaks are the deposited film and substrate, respectively. The $CaTiO_3$ layer is crystallized by heating the substrate during the deposition. This result indicates that substrate heating at 873 K is an appropriate technique for obtaining crystallized $CaTiO_3$ film.

XPS survey spectra for the deposited films contained the peaks originating from calcium, titanium, oxygen, and carbon. The origin of carbon was surface contamination adsorbed by exposure to the atmosphere. Typical XPS spectra for Ca 2p, Ti 2p, and O 1s regions are shown in Fig. 2. Results of peak fitting analysis with Gaussian–Lorentz function are also overlapped on the spectra. XPS spectra of Ca 2p and Ti 2p consist of two peaks, corresponding to doublet by spin–orbital splitting. The binding energy of the Ti $2p_{3/2}$ peak is 458.5 eV, indicating tetravalence titanium [16,19]. The binding energy of the Ca $2p_{3/2}$ peak is 346.9 eV, which is close to those of $CaTiO_3$, calcium hydroxide ($Ca(OH)_2$), and calcium oxide (CaO). It is reported that the binding energies of CaO and $Ca(OH)_2$ are slightly higher than that of $CaTiO_3$ [19]. However, these differences in the energies are too small to judge the chemical state. The XPS spectrum for the O 1s region is deconvoluted into three peaks, originating from anhydrous oxide (O^{2-}), the hydroxide group (OH^-), and adsorbed water (H_2O).

The atomic ratios of titanium to calcium ([Ti]/[Ca]) and atomic fractions of the hydroxide group ($[OH^-]/[O^{2-}]$) in the deposited films are plotted against the amount of oxygen gases, as shown in Fig. 3. In the reactive sputtering deposition (Fig. 3(a)), the [Ti]/[Ca] ratio of 1-sccm deposited film is lower than that of stoichiometric $CaTiO_3$. The [Ti]/[Ca] ratio increases and the $[OH^-]/[O^{2-}]$ ratio decreases with an increase of oxygen flow. The [Ti]/[Ca] ratio of the 10-sccm deposited film is ca. 1, which equals

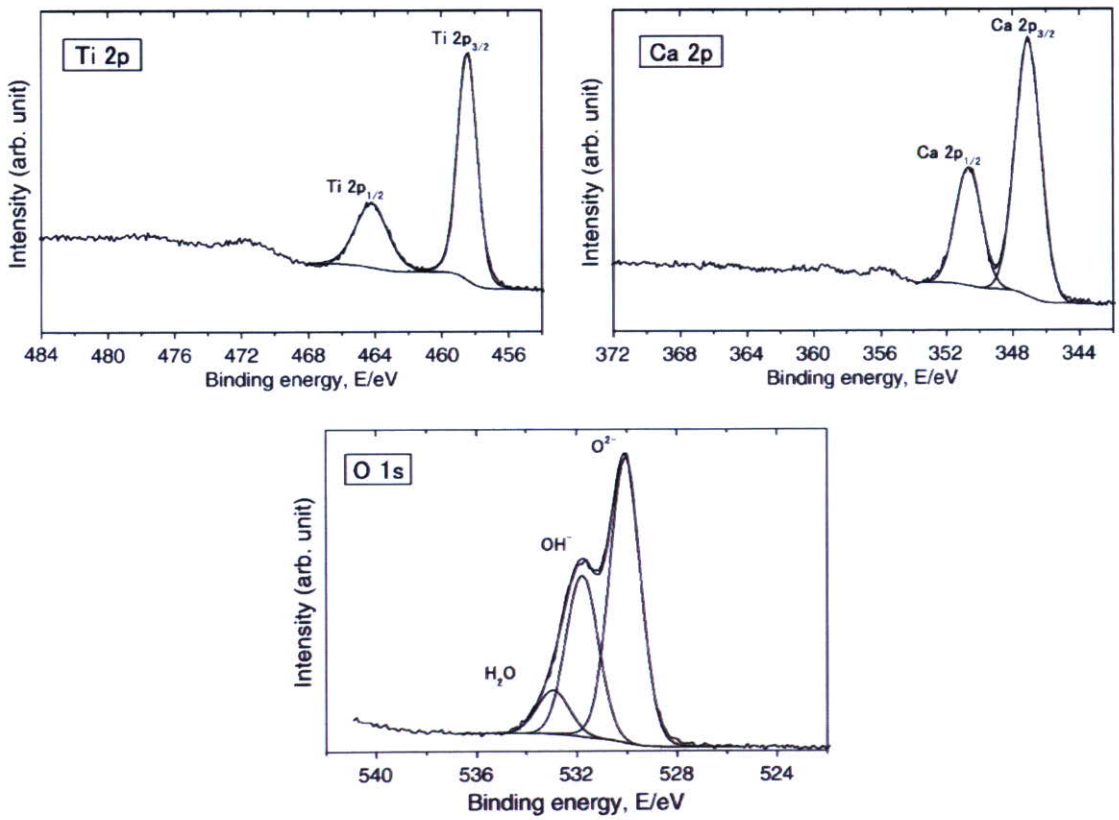

Fig. 2. XPS spectra of Ti 2p, Ca 2p, and O 1s regions for the $CaTiO_3$ film deposited by reactive sputtering with a 3-sccm oxygen flow. Results of peak fitting analysis with Gaussian–Lorentz function are also shown in the figures.

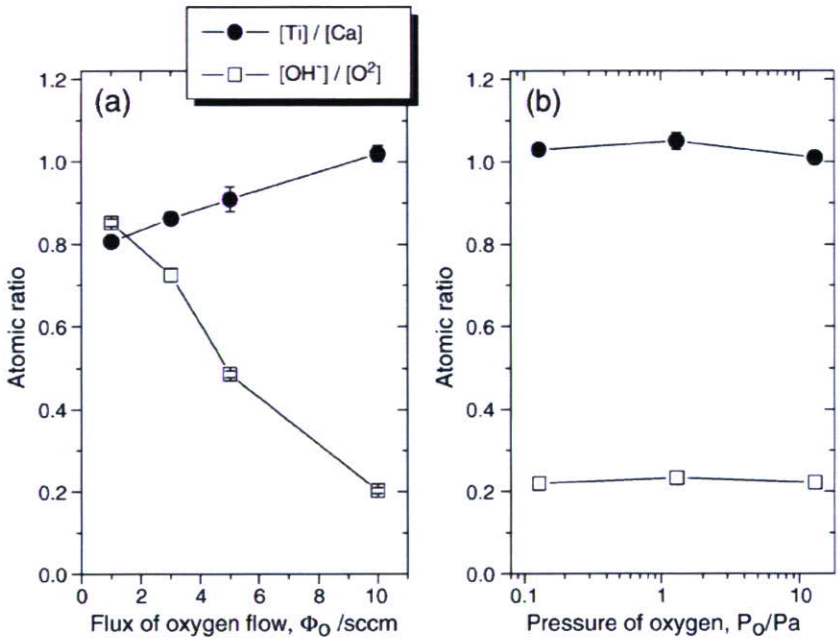

Fig. 3. Atomic ratios of titanium to calcium ([Ti]/[Ca]) and atomic fraction of hydroxide group ([OH^-]/[O^{2-}]) plotted against the amount of oxygen gases: (a) the $CaTiO_3$ films deposited by reactive sputtering, (b) the films deposited by pulsed laser deposition.

that of stoichiometiric $CaTiO_3$. On the other hand, in the pulsed laser deposition (Fig. 3(b)), the [Ti]/[Ca] ratio is almost constant at the oxygen pressure under the present experimental condition, and the value is ca. 1. Furthermore, the [OH^-]/[O^{2-}] ratio is also constant, and the value is almost in accordance with that of the film deposited by reactive sputtering with a 10-sccm oxygen flow. These results indicate that the characteristics of the $CaTiO_3$ film deposited by the reactive sputtering with a 10-sccm oxygen flow and the pulsed laser deposition with oxygen pressure in the range of 0.13 to 13 Pa are similar to each other.

3.2. Thickness of the oxide layer formed under $CaTiO_3$ thin film

Fig. 4 shows the typical depth profiles of Ca, Ti, and O for the $CaTiO_3$ film deposited on the titanium. The intensities of all signals are lower at the outermost surface due to the existence of contaminant carbon adsorbed in the air. The profiles show that the titanium-oxide layer is formed at the interface between the film and the titanium substrate.

The thicknesses of the titanium-oxide layers formed at the interface are shown in Fig. 5. Since real oxide layers may have

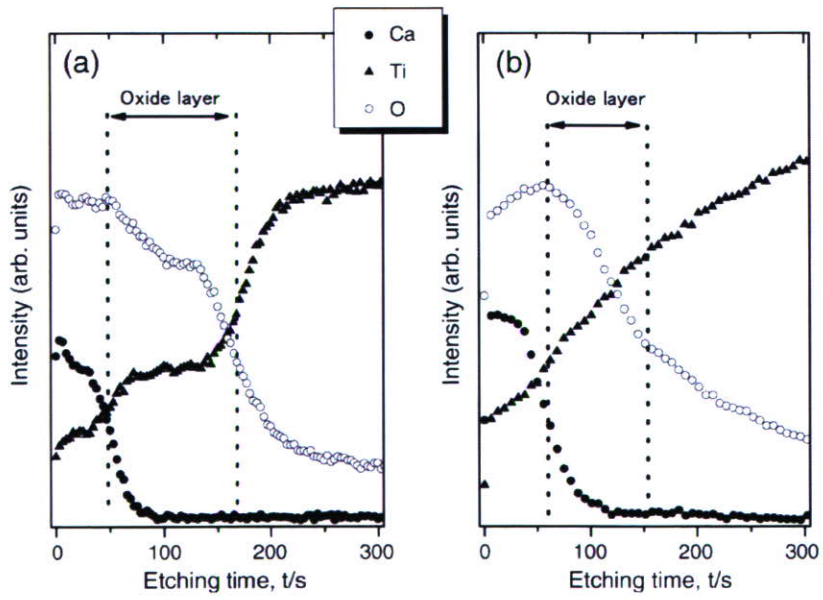

Fig. 4. Typical AES depth profiles of Ca, Ti, and O determined for the $CaTiO_3$ film deposited on titanium: (a) deposited by reactive sputtering with a 3-sccm oxygen flow, (b) deposited by pulsed laser deposition with oxygen pressure of 1.3 Pa.

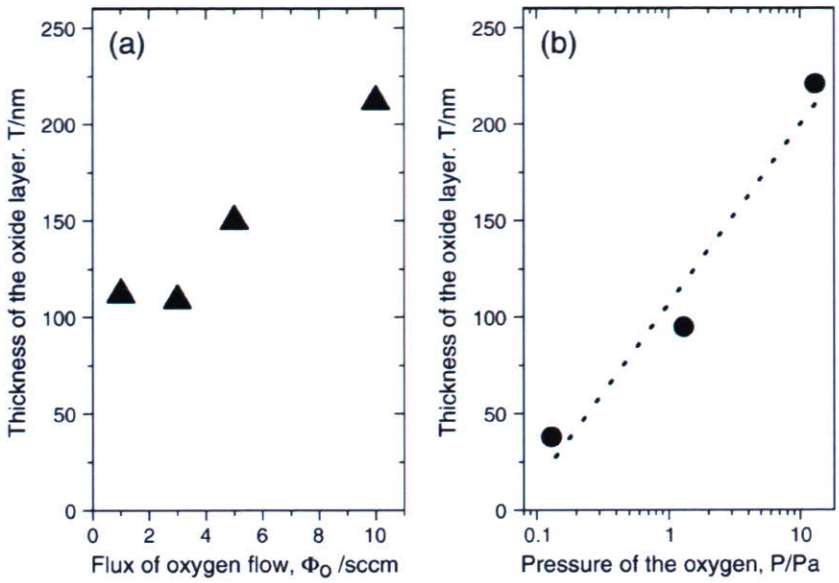

Fig. 5. Thicknesses of the titanium-oxide layer plotted against the amount of oxygen gases: (a) prepared by reactive sputtering, (b) prepared by pulsed laser deposition.

rough interface in the subnano-scale range, there is no clear boundary between the oxide layer and film or the substrate. In the present study, the titanium-oxide layer is defined as the region between the points where the intensities of Ca and O decrease to 50% in the depth profile. This definition is the same as that used in our previous study [15]. In the reactive sputtering deposition, the thickness of the oxide layer is almost constant up to a 3-sccm oxygen flow. Beyond a 3-sccm oxygen flow, the thickness increases with an increase of the oxygen flow. In order to obtain a $CaTiO_3$ film whose [Ti]/[Ca] ratio is equal to stoichiometric $CaTiO_3$, 10-sccm oxygen flow is necessary for preparation. Therefore, the formation of about a 220-nm thick titanium-oxide layer is unavoidable.

In the pulsed laser deposition, the thickness of the titanium-oxide layer is nearly proportional to the logarithm of the oxygen pressure ranging from 0.13 to 1.3 Pa. Since the stoichiometric $CaTiO_3$ film can be deposited with the oxygen pressure under the present experimental range, pulsed laser deposition makes it possible to form the stoichiometric $CaTiO_3$ thin film, the interface of which has a 40-nm oxide layer.

In comparison to the reactive sputtering and pulsed laser deposition techniques, it can be said that the pulsed laser deposition technique has an advantage in the formation of a stoichiometric $CaTiO_3$ thin film without a thick titanium-oxygen layer. This advantage is caused by the deposition rate. The deposition rate in the reactive sputtering deposition decreases with an increase of the oxygen flow [20], whereas the rate of the pulsed laser deposition is hardly changed. In the present study, the deposition rate of $CaTiO_3$ film by pulsed laser deposition was almost two times that by the reactive sputtering deposition with a 10-sccm oxygen flow.

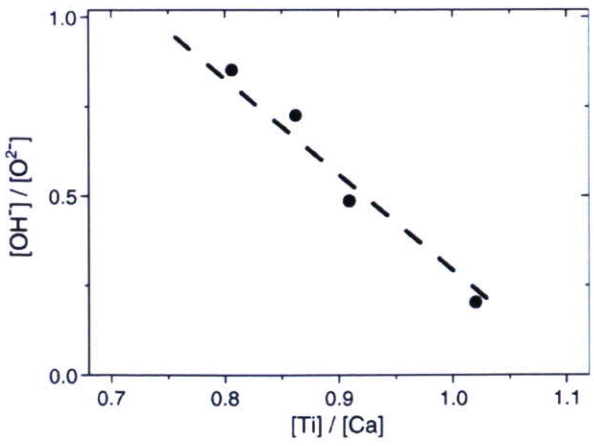

Fig. 6. Atomic fractions of hydroxide group ($[OH^-]/[O^{2-}]$) in the film deposited by reactive sputtering are plotted against the titanium-to-calcium ([Ti]/[Ca]) ratios.

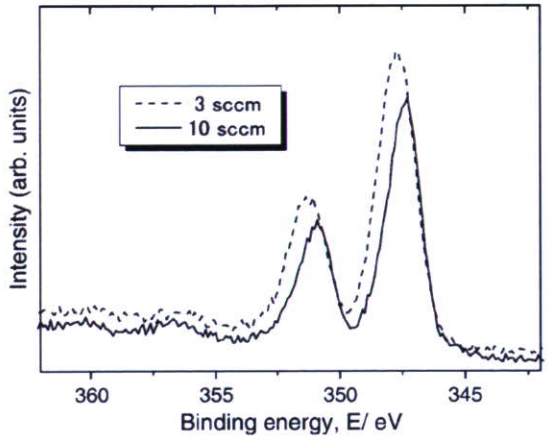

Fig. 7. Overlapping of the XPS spectra of the Ca 2p region for the film deposited by reactive sputtering with 3- and 10-sccm oxygen flows.

3.3. Relationship between the oxygen flow and film characteristics

In the reactive sputtering with oxygen flow in the range of 1 to 5 sccm, the [Ti]/[Ca] ratio of the deposited film was lower than that of stoichiometric $CaTiO_3$; in other words, calcium in the film is rich. Furthermore, in the Ca-rich films, the $[OH^-]/[O^{2-}]$ ratio is large. In Fig. 6, the $[OH^-]/[O^{2-}]$ ratios in the Ca-rich film are plotted against the [Ti]/[Ca] ratios. A good correlation between the [Ti]/[Ca] and $[OH^-]/[O^{2-}]$ ratios is observed. These results indicate that the Ca-rich film would contain not only $CaTiO_3$ but also $Ca(OH)_2$. The XPS spectra of the Ca 2p region for the film deposited with 3- and 10-sccm oxygen flows are overlapped in Fig. 7. It is clear that the peak width of the 10-sccm film is thinner than that of the 3-sccm film. Furthermore, the binding energy of Ca 2p peak for 10-sccm film is shifted to the lower energy side than that of 3-sccm film. The thinning of the Ca 2p peak and the shift of the binding energy are caused by the disappearance of $Ca(OH)_2$. These results provide direct support for $Ca(OH)_2$ formation in the Ca-rich film.

4. Conclusion

The $CaTiO_3$ thin films prepared by reactive sputtering and pulsed laser depositions are characterized by XPS, GI-XRD, and AES. The following conclusions are drawn:

1. In the reactive sputtering deposition, with an increase of oxygen flow, the titanium-to-calcium ratio of the deposited film approaches the ratio of stoichiometric $CaTiO_3$.
2. In the pulsed laser deposition, the titanium-to-calcium ratio is constantly near unity at the oxygen pressure in the range of 0.13 to 13 Pa.
3. In both deposition techniques, the crystallized $CaTiO_3$ film is obtained by heating the titanium substrate at 873 K, whereas the titanium-dioxide layer is formed at the interface between the film and the titanium substrate.
4. In both deposition techniques, the thickness of the titanium-dioxide layer increases with an increase of the amount of oxygen gases. The pulsed laser deposition has an advantage in formation of the stoichiometric $CaTiO_3$ film without formation of a thick titanium-oxide layer.
5. The film deposited by reactive sputtering with a low oxygen flow consists of calcium titanate and calcium hydroxide. The composition of calcium hydroxide decreases with an increase of the oxygen flow.

Acknowledgements

The authors gratefully acknowledge Prof. K. Asami for critically reviewing the manuscript. The authors are also grateful to Mr. Y. Murakami for supporting the AES measurement.

References

[1] K. Yamashita, E. Yonehara, X. Ding, M. Nagai, T. Umegaki, M. Matsuda, J. Biomed. Mater. Res. 43 (1998) 46.
[2] N. Yoshinari, Y. Ohtsuka, T. Derand, Biomaterials 15 (1994) 529.
[3] J.L. Ong, L.C. Lucas, Biomaterials 15 (1994) 337.
[4] K. van Dijk, H.G. Schaeken, J.G. Wolke, J.A. Jansen, Biomaterials 17 (1996) 405.
[5] Y.C. Tsui, C. Doyle, T.W. Clyne, Biomaterials 19 (1998) 2015.
[6] G. De Lange, C. De Putter, J. Oral Implantol. 19 (1993) 123.
[7] J.A. Jasen, J.P. van der Waerden, K. de Groot K, J. Biomed. Mater. Res. 25 (1991) 1535.
[8] H.W. Denissen, K. de Groot, P.C. Makkes, A. van den Hooff, P.J. Klopper, J. Biomed. Mater. Res. 14 (1980) 713.
[9] M. Jarcho, Clin. Orthop. 157 (1981) 259.
[10] K. De Groot, R. Geesink, C.P. Klein, P. Serekian, J. Biomed. Mater. Res. 21 (1987) 1375.
[11] R.G.T. Geesink, K. de Groot, C.P. Klein, J. Bone Jt. Surg. 70B (1988) 17.
[12] S.R. Radin, P. Ducheyne, J. Mater. Sci., Mater. Med. 3 (1992) 33.
[13] R.G.T. Geesink, K. de Groot, C.P. Klein, Clin. Orthop. 225 (1987) 147.
[14] K. Asami, K. Saito, N. Ohtsu, S. Nagata, T. Hanawa, Surf. Interface Anal. 35 (2003) 483.
[15] N. Ohtsu, K. Saito, K. Asami, T. Hanawa, Surf. Coat. Tech. 200 (2006) 5455.
[16] N. Ohtsu, K. Sato, K. Saito, K. Asami, T. Hanawa, J. Mater. Sci., Mater. Med. (in press).
[17] N. Ohtsu, K. Sato, A. Yanagawa, K. Saito, Y. Imai, T. Kohgo, A. Yokoyama, K. Asami, T. Hanawa, J. Biomed. Mater. Res. (in press).
[18] S. Kobayashi, T. Inoue, K. Nakai, Mater. Trans. 46 (2005) 207.
[19] T. Hanawa, H. Ukai, K. Murakami, J. Electron Spectrosc. Relat. Phenom. 63 (1993) 347.
[20] T. Narushima, K. Ueda, T. Goto, H. Masumoto, T. Katsube, H. Kawamura, C. Ouchi, Y. Iguchi, Mater. Trans. 46 (2005) 2246.